Compact Fluorescent Lamps phase dependency modelling and harmonic assessment of their widespread use in distribution systems

Zhiliang Wei (B.E. Hons)

A thesis submitted in partial fulfilment
of the requirements for the degree of
Master of Engineering
in
Electrical and Computer Engineering
at the
University of Canterbury,
Christchurch, New Zealand.

September 2009

ABSTRACT

This thesis presents the research on CFL's phase dependency modelling to provide an improved harmonic assessment of their widespread use in distribution system. Conventionally, CFL is modelled as fixed harmonic current source, which ignores the harmonic interaction with the ac electrical network. However, with different magnitude and phase angle of the applied voltage, CFL's harmonic current injection will be varied. This leads to the methodology of using a Norton equivalent circuit to model CFL's harmonic behaviour.

In a small voltage distortion range, such as 5% V_{THD}, the CFL admittance is phase dependent with the phase angle of the applied voltage. This dependency character is described by tensors, which are widely used in physics to represent the invariant relationship between vectors under rotation of coordinate axes. Two methods are purposed to find the optimal value of the linearized admittance tensors on a perturbation level of 3.26% of V_{THD}. The first method is to average the tensor results from the original admittance plots based on select points. In the second method, the admittances are rearranged into one double traced circle, and then find the linearized admittance tensor. Both methods show strong agreement and good validity. This also provides an opportunity to analyze the harmonic behaviour of small rating nonlinear electronic devices from a new prospective.

This proposed CFL model is applied to a typical New Zealand distribution network with comparison of using conventional fixed harmonic current source approach. The V_{THD} caused by large quantity of CFLs is given a more realistic "worst case" scenario. The harmonic interference with ripple control system is also discussed.

ACKNOWLEDGEMENTS

Firstly, I would like to thank my supervisor Professor Neville Watson for his trust, encouragement, and patient guidance. Thank David Smith, and Lance Frater for their assistance and discussion at the beginning of this research.

Many thanks should also go to the rest of the A215ers and friends for the refreshing conversions and outdoor activities to keep my mind out of the circles. I would also like to acknowledge the financial support I received through the Departmental Research Funding as well as the Electric Power Engineering Centre (EPEC) Postgraduate Scholarship.

Finally, to my family for their love and support. To them I dedicate this thesis.

CONTENTS

LIST OF FIGURES

LIST OF TABLES

GLOSSARY

Abbreviations

CFLs	Compact Fluoresent Lamps
DF	Distortion Factor
DPF	Displacement Power-Factor
GXP	Grid eXit Point
HPA	Harmonic Perturbation Analysis
kV	kilo-Volts
LV	Low Voltage
OHL	Overhead Lines
PSCAD	Power System Computer Aided Design - Interface for EMTDC
THD	Total Harmonic Distortion
UGC	Underground Cables

Symbols

V, I	Voltage, Current
V_{THD}	Total harmonic voltage distortion
I_{THD}	Total harmonic current distortion
V_n, I_m	n^{th} order harmonic voltage, m^{th} order harmonic current
$V_{n,perturbed}$	n^{th} order harmonic voltage perturbation
I_{base}	Harmonic current components at base case
ΔV_n	n^{th} order harmonic voltage variation
ΔI_m	m^{th} order harmonic current variation
Y	Admittance
Y_{CFL}	CFL admittance matrix
$Y_{m,n}$	Frequency coupling between ΔV_n and ΔI_m
Y_{system}	System admittance matrix
$Y_{k,k}$	Self-admittance at node k
$Y_{k,l}$	Mutual-admittance between node k and node l

Chapter 1

INTRODUCTION

1.1 MOTIVATION OF THE RESEARCH

The increasing demand of electricity leads to the expansion of generation and transmission capacity to meet the future needs. At the same time, the local utilities have also encouraged the customers to use electricity during off-peak hours and promoted the energy saving equipment to use electricity more efficiently.

However, the large quantities of these energy efficient devices used in residential and commercial areas usually have truncated sinusoidal current waveforms, and their individual harmonic filtering are often "neglect". Thus, the widespread use of these small rating nonlinear loads has become significant harmonic sources in the electrical network, and the quality of these electrical appliances are becoming a major influencing to the V_{THD} in the medium and low voltage feeders in the near future.

One of these devices frequently addressed in numerous research papers and reports is the discharging lamps in particular the modern Compact Fluorescent Lamps (CFLs) with electronic ballasts. This is also the area of consideration in this thesis.

1.2 METHODOLOGY OF HARMONIC ANALYSIS

Detailed modelling of the generation, summation and propagation of harmonics is required at the power system planning level to ensure the harmonic levels are within the regulator limits. The methods for performing the harmonic analysis can be summarized into the following four categories:

Fixed harmonic current source

This approach assumes that the CFL harmonic current injection is fixed regardless of the voltage distortion on the supply. This method has been widely recognized [1] to present the worst case scenario for design purpose. However, its drawback is the limited accuracy as it is often proven to be too conservative in most practical applications due to the fact that harmonic phasors may have significant differences in phase angle particular at higher harmonics (11^{th} and beyond).

Statistic approach (Probability modelling/ Monte Carlo simulation)

The current waveform drawn from the nonlinear devices consists of a series of harmonic components of different orders. For the same type of nonlinear load with different topology, their lower harmonic components usually have a similar phase angle. As a result, the arithmetic sum of these harmonic vectors will give a closed match with actual summation between vectors. However, as these nonlinear loads connected in parallel to the same voltage feeder, their actual total harmonics will reduce as the number of nonlinear loads increases due to the shared impedance [2]. For higher harmonic order phasors, their phase angles become more diverse due to the nature of their circuit topology (slightly different current waveform drawn). Therefore, their resultant harmonic phasors often drop more dramatically due to both attenuation and diversity nature.

For the nonlinear loads with different functionality (e.g. adjustable speed drive and battery charger), the harmonic phasors will be more random because of the diversity in operation. Therefore, the overall harmonics from these nonlinear loads will result a random magnitude and phase angle from time to time. Some researchers [3, 4] have proposed the method of using probabilistic model and Monte Carlo simulation to calculate the summation of these harmonic current and voltage phasors. However, the limitation of this statistic approach is the reliability and accuracy of these statistic data and the lack of modelling on the interaction between the harmonic voltage and current of the nonlinear loads.

Iterative harmonic analysis

In order to model these harmonic interactions in detail, the mathematical model of the nonlinear load is included in the active and reactive power-flow equations for the balanced [5] and unbalanced [6] three phase system to obtain their voltage and current harmonic components through an iterative harmonic analysis. Although some researchers [7, 8, 9, 10] have proposed few mathematical models for the mercury discharging lamps (including modern CFLs), no further studies have been performed using IHA for their harmonic assessment. This is mainly due to their sophisticated mathematical model as well as much lower power rating, with its widespread deployment nature, compared to three-phase rectifier loads and large rating power electronic converters.

Frequency domain linearization

To overcome these deficiencies, this thesis proposes a method of using Norton equivalent circuit to model CFL in the harmonic (frequency) domain. The linearized CFL admittance is taken into account as part of the system admittance matrix. Through a direct harmonic analysis, the incremental voltage distortion can be determined in one nodal equation. This method is more suitable for CFL as it usually has constant conducting period and relatively stabilized waveform around a base operating point as compared to adjustable speed drives and battery chargers. It

also provides more detailed and accurate results in terms of voltage distortion at the medium and low voltage feeders compared to the three methods mentioned above.

1.3 AIM OF RESEARCH

The harmonic currents injected by a CFL depend on the voltage harmonics, particularly their angles, at its terminals. However, to date fixed harmonic current sources have been used in studies to determine the effect of CFLs on an electrical distribution network, and this does not model the dependency of the harmonic current of the voltage harmonics (called phase-dependency). Therefore, the main aim of this research is to assess how significant this phase dependency is by redoing an earlier study that looked at the impact of large scale deployment of CFLs, using a model that represents the CFL more accurately and comparing to the results from using the fixed harmonic current injection. In order to achieve this goal, several sub goals need to be obtained:

1. Determine the phase dependency of a typical CFL. This will be achieved by perturbation analysis using a detailed electromagnetic transient program with the relevant CFL ballast circuitry modelled.

2. Develop a suitable model for assessing the effect of the widespread deployment of CFLs on an electrical distribution network that represents the phase-dependency adequately. The harmonic domain will be chosen as the framework and the CFLs need to be represented by harmonic tensors.

3. A harmonic domain algorithm needs to be written for the system being studied and the CFL model incorporated into this.

1.4 THESIS OUTLINE

Chapter 2: Background This chapter provides the basis of harmonic modelling of CFL. It explains the methodology used for CFL linearization as well as the solution of finding its harmonic interaction with the ac electrical network.

Chapter 3: Harmonic modelling of compact fluorescent lamps This chapter implements the CFL linearization under a wide range of voltage distortion, and describes how the CFL admittance tensors are determined, this is followed by the validation of the proposed model.

Chapter 4: Case study: Harmonic assessment of widespread use of CFLs in a distribution system In this Chapter, the CFL harmonic model developed in Chapter 3 is applied to a typical New Zealand distribution network to quantify the harmonic impact of their widespread use. The harmonic interference with ripple control system is also discussed.

Chapter 5: Conclusions and future work This chapter summarizes the research described by this thesis. The future extension of this research is also discussed.

1.5 PUBLICATION

One publication has resulted from this research work: Z.Wei, N.R. Watson, and L.P. Frater, "Modelling of compact fluorescent lamps," *Proceedings of* 13^{th} *ICHQP*, October 2008.

Chapter 2

BACKGROUND

2.1 INTRODUCTION

The term *Power Quality* refers to how close the voltage waveform is to the ideal sinusoidal waveform. One of the main power quality problems is the steady-state distortion, which is quantified by the harmonic components of the waveform. The detrimental effects of harmonics are numerous and well documented in the literature [11].

Harmonics appeared early in the development of electrical power systems in the form of slot harmonics from electrical machines and due to saturation in transformers. However, with the development of mercury-arc converter and later thyristor converters, the magnitude of the harmonic sources in the system greatly increased. In the New Zealand context the inter-Island HVdc link and Aluminium Smelter at Tiwai were the two largest harmonic sources which have drawn the most attention for harmonic analysis. With large harmonic sources such as these it is a simple task to provide harmonic filters.

The dramatic development of technology has resulted the reduction in the cost of solid state devices and its wide use for the control of power at all levels. At the high power levels, besides the HVdc links, FACTS devices are being used to control power in HV electrical network. At the medium power level, there are numerous variable speed drives (both ac and dc drives) being deployed for a wide variety of applications such as irrigation pumps, printing presses and gondolas.

The drive for energy efficiency has also led to the field of low power electronic devices. Recently, the New Zealand Government and electricity companies have been encouraging the use of CFLs as part of a national energy saving programme. However, CFL utilizes a single-phase rectifier followed by capacitor filter, and the current waveform it draws from the electrical network is very rich in harmonics. Until recently, harmonics from CFLs have been ignored due to their very low power ratings as compared to other harmonic producing loads. However, now that CFLs are being deployed in their millions, collectively their impact can result in unacceptable power quality.

To avoid electrical equipment having a detrimental effect on other equipment connected to the system, standards and regulations are required. New Zealand was one of the first countries to

issue regulations to limit harmonic levels with the *Limitation of Harmonic Levels Notice 1981* issued by the Office of the Chief Electrical Inspector (Ministry of Commerce). This has been embodied in the present NZECP 36:1993 [12] (New Zealand Electrical Code of Practice for Harmonic Levels) cited by Electrical Regulations. The joint Australia/ New Zealand standard AS/NZS 61000.3.2 [13] sets the allowable harmonic voltage distortion for distribution system and the acceptable harmonic injection levels for equipment whose input current is equal or less than 16 Amperes per phase. At present this is a voluntary standard.

2.2 HARMONIC MODELLING

2.2.1 General

Power system harmonics is a steady-state phenomenon, and the voltage and current can be determined in either the time or frequency domain. Harmonic analysis in the time domain involves setting up differential equations to represent the dynamics of the system, and then uses numerical integration to solve the equations. The calculated current and voltage are at discrete time points. Time domain simulation software packages such as PSCAD/EMTDC, ATP/EMTP and PSPICE involve simulation to steady-state and then use FFT to present the data in the form of their frequency spectra. Previously, time domain simulation on CFLs often concentrates on the detailed modelling of their internal electronic ballast design to improve the energy efficiency and power-factor of CFLs at minimum cost [14, 15, 16, 17]. More recently, some researchers [10] have also used PSPICE as a time domain simulation tool to characterize the current waveform drawn under a series of voltage supply with different magnitudes. It helps to analyze the changes of CFL harmonic current injection due to the variation of the supply voltage, which is especially important for weak electrical network. Lately, a study using PSCAD/EMTDC was conducted to model a distribution network supplied by photovoltaic station in one of the islands in Greek island. With different percentages of CFLs loading modelled as fixed harmonic current source, the results show that the large scale use of CFLs can cause over 20% V_{THD} rise in most of the busbars in that particular weak system [18].

Compared with time domain simulation, harmonic analysis in the frequency domain has the advantage of computational efficiency. The principle of superposition is applied to enable each harmonic frequency to be considered separately [19]. The differential equations are converted to complex algebraic equations represented by complex phasor either in rectangular or polar form, which are easier for incorporating the frequency dependent behaviour of components. An extension of the frequency domain is the harmonic domain. It models the harmonic interactions from the fundamental frequency up to the highest harmonic order of interest in one matrix equation, including the control system [20]. Traditionally, CFL is modelled as fixed harmonic current source, as shown in Figure 2.1(a), which ignores the harmonic interaction with the ac electrical network. However, with different magnitudes and phase angles of the supply voltage, the CFL harmonic current injection will be varied. This leads to the methodology of adding

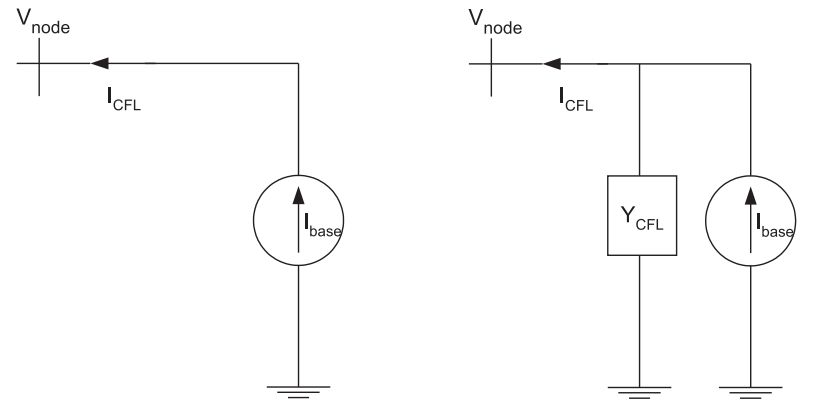

Figure 2.1 CFL harmonic representations

CFL admittance information to represent CFL as a Norton equivalent circuit, as shown in Figure 2.1(b). With the addition of system admittance, the harmonic voltage distortion at each busbar can be calculated. It also provides a more comprehensive solution in terms of the harmonic attenuation and resonance effects as comparing to the fixed harmonic current source.

2.2.2 CFL Norton equivalent representation

CFL linearization

Due to the nonlinear character of CFL, a small voltage variation at one frequency causes the change of current components of many frequencies. This results the CFL admittance matrix in a frequency cross-coupling manner. The CFL admittance can be described as a frequency response between the input signal (voltage) and output signal (current), and the coupling between them in a small linear region around the operating point yields a constant admittance value. In reality the supply voltage of a CFL will not be pure sinusoidal, and the presence of voltage distortion can be modelled through harmonic perturbation analysis [21]. This is achieved by superimposing the harmonic voltage distortion ΔV_h to the CFL to obtain the resulting ΔI_h. It provides an opportunity to transform the time domain nonlinear characteristic into a linear frequency domain. Due to the small magnitude of ΔV_h, each perturbation is considered as a linear operation, whose first partial derivatives remain approximately the same as the unperturbed base case at that operating point. In general, the coupling between n^{th} order harmonic voltage and m^{th} order harmonic current can be expressed as:

$$Y_{m,n} = \frac{\partial I_{m,perturbed}}{\partial V_{n,perturbed}} = \frac{I_{m,perturbed} - I_{m,base}}{V_{n,perturbed} - V_{n,base}} = \frac{\Delta I_m}{\Delta V_n} \tag{2.1}$$

Although $Y_{m,n}$ varies with the magnitude and phase angle of the applied voltage, with a small distortion such as ΔV_h, $Y_{m,n}$ is phase dependent with an invariant magnitude. The overall

linearized CFL admittance matrix can be obtained by combining all these first partial derivatives into one matrix, and is usually represented either in complex-conjugated [22] or real-valued tensor form [23]:

$$Y_{CFL} = \begin{bmatrix} \frac{\partial I_1}{\partial V_1} & \frac{\partial I_1}{\partial V_3} & \frac{\partial I_1}{\partial V_5} & \cdots & \frac{\partial I_1}{\partial V_m} & \cdots & \frac{\partial I_1}{\partial V_n} \\ \frac{\partial I_3}{\partial V_1} & \frac{\partial I_3}{\partial V_3} & \frac{\partial I_3}{\partial V_5} & \cdots & \frac{\partial I_3}{\partial V_m} & \cdots & \frac{\partial I_3}{\partial V_n} \\ \frac{\partial I_5}{\partial V_1} & \frac{\partial I_5}{\partial V_3} & \frac{\partial I_5}{\partial V_5} & \cdots & \frac{\partial I_5}{\partial V_m} & \cdots & \frac{\partial I_5}{\partial V_n} \\ \vdots & \vdots & \vdots & \ddots & \vdots & & \vdots \\ \frac{\partial I_m}{\partial V_1} & \frac{\partial I_m}{\partial V_3} & \frac{\partial I_m}{\partial V_5} & \cdots & \frac{\partial I_m}{\partial V_m} & \cdots & \frac{\partial I_m}{\partial V_n} \\ \vdots & \vdots & \vdots & & \vdots & \ddots & \vdots \\ \frac{\partial I_n}{\partial V_1} & \frac{\partial I_n}{\partial V_3} & \frac{\partial I_n}{\partial V_5} & \cdots & \frac{\partial I_n}{\partial V_m} & \cdots & \frac{\partial I_n}{\partial V_n} \end{bmatrix} \tag{2.2}$$

Representations of CFL admittance matrix

In the process of CFL linearization, one complex number is not able to represent its admittance variation due to the phase dependency. This often requires two complex numbers to incorporate dependency on the harmonic voltage phasor. Traditionally, the linearization has been carried out by representing harmonic vectors ΔI and ΔV with both positive and negative frequency terms, which lead to a complex-conjugated admittance matrix as shown in Equation 2.3.

$$\left[\begin{array}{c} \Delta I_+ \\ \hline \Delta I_- \end{array}\right] = \left[\begin{array}{c|c} Y_1 & Y_2 \\ \hline Y_1^* & Y_2^* \end{array}\right] \left[\begin{array}{c} \Delta V_+ \\ \hline \Delta V_- \end{array}\right] \tag{2.3}$$

However, the linearization using two complex numbers Y_1 and Y_2 related to positive frequency term is capable of describing the overall linear transformation in a real-valued manner as:

$$\Delta I_+ = Y_1 \Delta V + Y_2 \Delta V^* \tag{2.4}$$

Decomposing this into real and imaginary part of the positive frequency components yields:

$$(I_r + jI_i) = (Y_{1r} + jY_{1i})(V_r + jV_i) + (Y_{2r} + jY_{2i})(V_r - jV_i) \tag{2.5}$$

$$I_r = (Y_{1r}V_r - Y_{1i}V_i) + (Y_{2r}V_r + Y_{2i}V_i) \tag{2.6}$$

$$I_i = (Y_{1r}V_i + Y_{1i}V_r) + (-Y_{2r}V_i + Y_{2i}V_r) \tag{2.7}$$

$$\begin{bmatrix} \Delta I_r \\ \Delta I_i \end{bmatrix} = \begin{bmatrix} Y_{11} & Y_{12} \\ Y_{21} & Y_{22} \end{bmatrix} \begin{bmatrix} \Delta V_r \\ \Delta V_i \end{bmatrix} \tag{2.8}$$

CFL phase dependency

The linearized CFL admittance depending on the phase angle of the supply voltage can be simulated through a particular harmonic perturbation analysis. For instance, Figure 2.2 displays the loci of ΔV_3 as its angle changes from 0 to 360 degree with magnitudes of 0.05%, 0.10% and 0.15% of fundamental voltage respectively. By applying all these different voltage perturbations

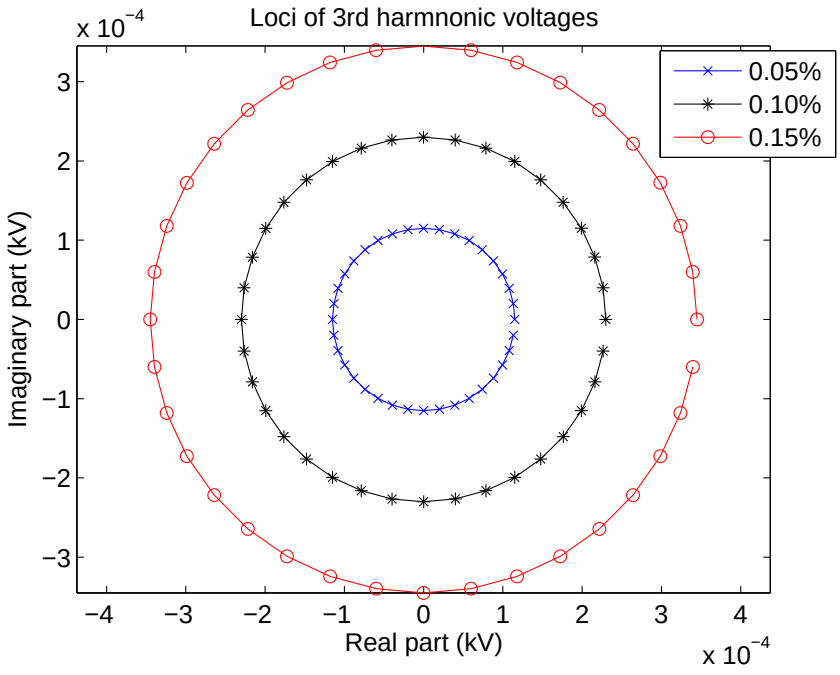

Figure 2.2 Loci of ΔV_3 at 0.05%, 0.10% and 0.15% of fundamental voltage

separately, the corresponding ΔI_3 vary in the elliptical manner as shown in Figure 2.3. By using Equation 2.1, all the corresponding CFL admittances $Y_{3,3}$ are calculated and plotted in Figure 2.4. During each perturbation as the phase angle of the ΔV_3 varies in a complete circle, the CFL admittance changes in a double traced circular form due to the sum of phase angles from both positive and negative frequency terms. Figure 2.4 also indicates that all these three levels of voltage perturbations are within the linear region around the fixed operating point, as the admittance $Y_{3,3}$ has the same locus during each perturbation. Figure 2.5 further illustrates this by displaying more phase dependent cross-coupling admittances for a CFL at 0.1% voltage distortion. This phase dependent behaviour of the CFL admittance can be described using a 2^{nd} rank tensor [24], which requires four real valued unknowns Y_{11}, Y_{12}, Y_{21} and Y_{22}. When the CFL is fully linearized, only two harmonic perturbation points $(\Delta V_3(1), \Delta I_3(1))$ and $(\Delta V_3(2), \Delta I_3(2))$ are needed to solve these four unknowns $\begin{bmatrix} Y_{11} & Y_{12} \\ Y_{21} & Y_{22} \end{bmatrix}$ simultaneously [25] as shown in Equation 2.9.

$$\begin{bmatrix} \Delta I_r(1) \\ \Delta I_i(1) \\ \Delta I_r(2) \\ \Delta I_i(2) \end{bmatrix} = \begin{bmatrix} \Delta V_r(1) & \Delta V_i(1) & 0 & 0 \\ 0 & 0 & \Delta V_r(1) & \Delta V_i(1) \\ \Delta V_r(2) & \Delta V_i(2) & 0 & 0 \\ 0 & 0 & \Delta V_r(2) & \Delta V_i(2) \end{bmatrix} \begin{bmatrix} Y_{11} \\ Y_{12} \\ Y_{21} \\ Y_{22} \end{bmatrix} \tag{2.9}$$

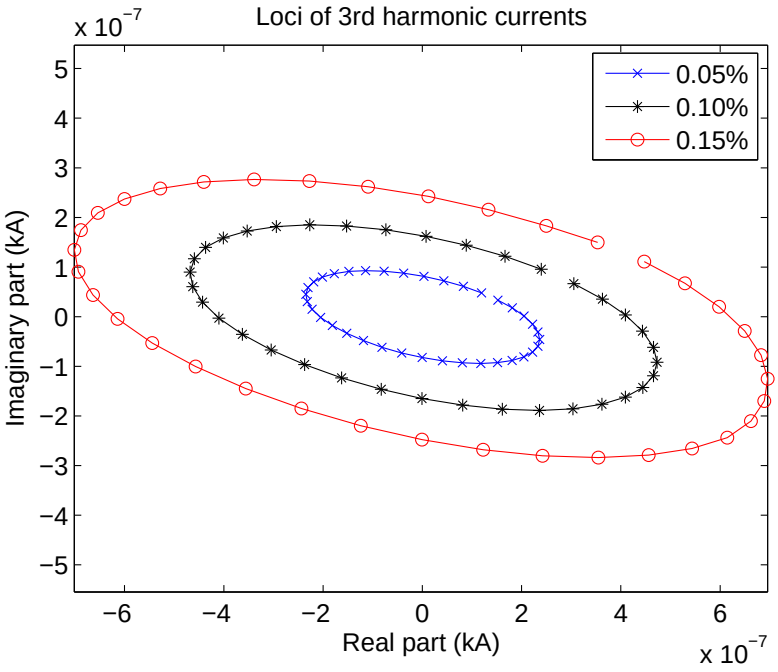

Figure 2.3 Loci of ΔI_3 at 0.05%, 0.10% and 0.15% voltage distortions

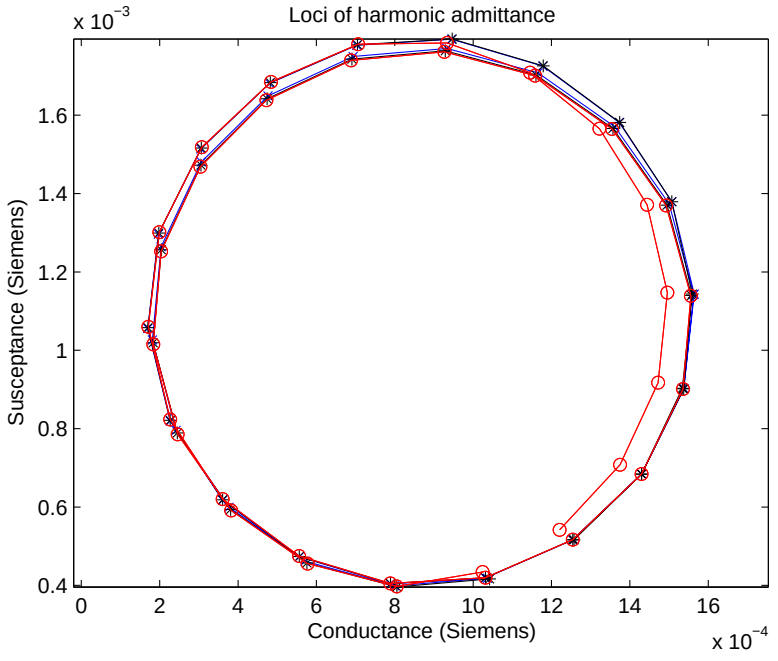

Figure 2.4 Loci of $Y_{3,3}$ at 0.05%, 0.10% and 0.15% voltage distortions

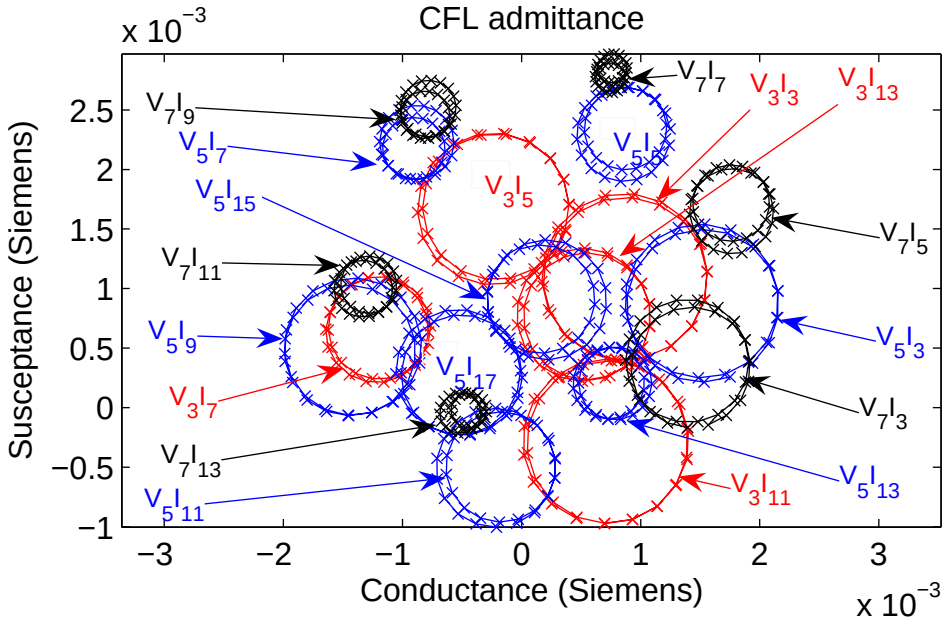

Figure 2.5 Loci of various phase dependent cross-coupling admittances at 0.1% voltage distortion

As a result, the extended form of the linearization at all frequencies can be written as:

$$\begin{bmatrix} \Delta I_1 \\ \Delta I_3 \\ \Delta I_5 \\ \vdots \\ \Delta I_m \\ \vdots \\ \Delta I_n \end{bmatrix} = \begin{bmatrix} Y_{1,1} & Y_{1,3} & Y_{1,5} & \cdots & Y_{1,m} & \cdots & Y_{1,n} \\ Y_{3,1} & Y_{3,3} & Y_{3,5} & \cdots & Y_{3,m} & \cdots & Y_{3,n} \\ Y_{5,1} & Y_{5,3} & Y_{5,5} & \cdots & Y_{5,m} & \cdots & Y_{5,n} \\ \vdots & \vdots & \vdots & \ddots & \vdots & & \vdots \\ Y_{m,1} & Y_{m,3} & Y_{m,5} & \cdots & Y_{m,m} & \cdots & Y_{m,n} \\ \vdots & \vdots & \vdots & \ddots & \vdots & & \vdots \\ Y_{n,1} & Y_{n,3} & Y_{n,5} & \cdots & Y_{n,m} & \cdots & Y_{n,n} \end{bmatrix} \begin{bmatrix} \Delta V_1 \\ \Delta V_3 \\ \Delta V_5 \\ \vdots \\ \Delta V_m \\ \vdots \\ \Delta V_n \end{bmatrix} \tag{2.10}$$

where every $Y_{m,n}$ is a 2×2 tensor with four real-valued elements, and each ΔI and ΔV are expressed as a 2×1 vector to represent both real and imaginary part of positive frequency harmonic phasor.

CFL harmonic interaction

The harmonic interaction between CFLs and the ac electrical network depends on the quantity of their harmonic current injections, the structure of the electrical network as well as the presence of other loads connected to the system. Generally, the quality of the supply voltage affects the CFL harmonic current injection, which also in turn influences the terminal voltage distortion as illustrated in Figure 2.6. The cross-coupling admittance matrix combining with its harmonic

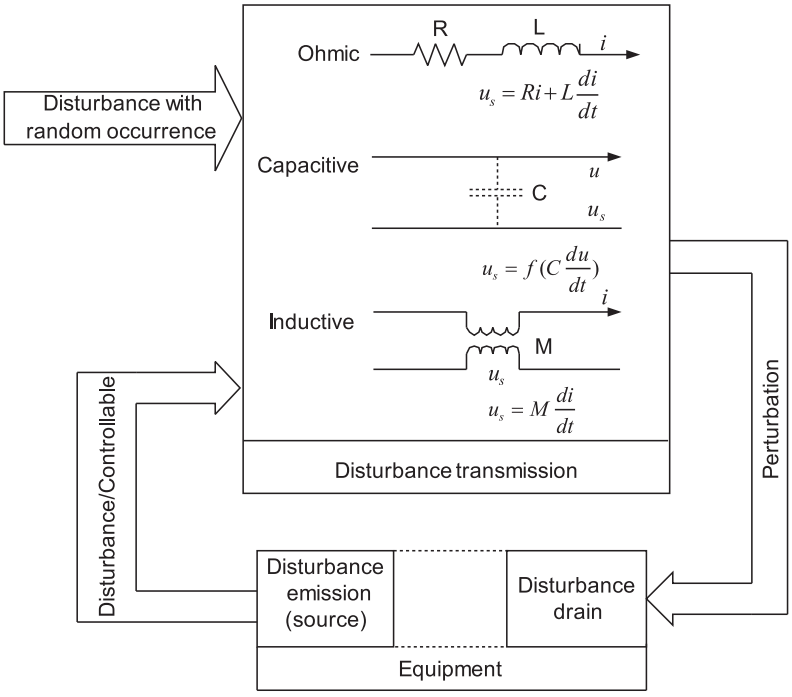

Figure 2.6 Basic relation of harmonic current emission, interaction and coupling of disturbances [26]

current injections at the base case is able to model such harmonic interaction between CFL and the ac electrical network in detail. This is achieved by finding the CFL harmonic current injection from the base operating point (V_{base} distortion-free), and then using the system admittance matrix to calculate the voltage distortion ΔV_{node}. This incremental voltage distortion is then added to the network background voltage distortion $V_{harbase}$ to calculate the variation of CFL harmonic current injection ΔI_{node}, as part of the I_{base} is flowing into the ground through its shunt admittance. As a result, the actual CFL harmonic current injection and overall voltage distortion at the terminal can be determined. The whole process is shown in Equation 2.11-2.14.

$$\Delta V_{node} = [Y_{system}]^{-1} I_{base} \tag{2.11}$$

$$\Delta I_{node} = [Y_{CFL}](V_{harbase} + \Delta V_{node}) \tag{2.12}$$

$$I_{CFL} = I_{base} - \Delta I_{node} \tag{2.13}$$

$$V_{node} = V_{base} + V_{harbase} + \Delta V_{node} \tag{2.14}$$

2.3 CONCLUSIONS

The chapter has briefly reviewed the existing harmonic modelling techniques on CFLs, and also examined the proposed method (described in Chapter 1) to model CFL's external harmonic behaviour. The CFL linearization is obtained through harmonic perturbation analysis with variable phase angles, and this leads to the use of tensors to describe CFL's phase dependent

admittances in a real-valued manner. More specific examples using this harmonic technique applied to CFLs will be detailed in Chapter 3.

Chapter 3

HARMONIC MODELLING OF COMPACT FLUORESCENT LAMPS

3.1 INTRODUCTION

Compact fluorescent lamps were initially introduced to the customers in the 1980s as an alternative for the incandescent lamps. Due to the negative resistive character of the fluorescent lamp, a ballast is required to limit the current flowing into the lamp. This was achieved by using a magnetic coil in series with the lamp to serve as a high impedance load. The inductive magnetic coil causes a DPF (displacement power-factor) issue, and is also responsible for both generation and limitation of the harmonic currents. In modern CFL design the magnetic ballast is replaced by solid state devices to create a higher frequency ac voltage supply to the lamp. It improves the power efficiency of the lamp and also removes most of the light flicker. However, the small conduction period of the rectifier and capacitor filter combination creates rich harmonics, which causes a poor DF (distortion factor).

3.2 BACKGROUND

3.2.1 Power-Factor

Power-factor is a key measure of utilization of a network. In a linear system (distortion free), the power-factor known as DPF is only determined by the phase difference between voltage and current. However, the power-factor of a nonlinear device like CFL, which has a distorted current waveform, should include its harmonic frequency components. Thus the whole expression of power-factor is the product of DPF and DF as derived in Equation 3.1.

$$\begin{aligned} PF &= \frac{Active\ Power}{Total\ Apparent\ Power} = \frac{\frac{1}{T}\int_0^T vi\,\mathrm{d}(t)}{V_{RMS}I_{RMS}} = \frac{\sum_{i=1}^{n} V_n I_n \cos\phi_n}{V_{RMS}I_{RMS}} \approx \frac{V_1 I_1 \cos(\phi_1)}{V_1 I_{RMS}} \\ &= \frac{I_1}{I_{RMS}} \times \cos\phi_1 = DP \times DPF \end{aligned} \tag{3.1}$$

Many CFLs sold in New Zealand market have power-factor between 0.44 and 0.60 with DF typicallyg around 0.50. Such low power-factor reduces CFL's energy efficiency as its apparent power drawn could be twice the rated power. It also brings the burden to the electrical network due to their high percentage of harmonic current injections.

3.2.2 CFL harmonic performance and its power-factor correction

Figure 3.1 displays a typical CFL ballast circuit, and is divided into four blocks for analysis purpose. The 1^{st} block usually has the protection, filtering and current peak limiting components. It attenuates the electromagnetic interference generated by the high frequency stages of the ballast, and also protects the ballast against possible transient phenomenon. The 2^{nd} block is the ac/dc conversion using full-bridge diode rectifier. This is followed by a capacitor in block 3 to provide a smooth dc voltage for the resonant inverter in block 4. The lamp is supplied by a resonant inverter started by the DIAC, and self-oscillating between 10 and 40 kHz. It also provides a high voltage to strike across the tube. However, in order to prolonging the tube life, PTC is recommended, to be placed in parallel with the tube, to extend the pre-heat stage. Generally the lamp appears as a constant resistive load as far as the dc busbar is concerned. The first three blocks have enormous impact on the CFL harmonic performance. CFL can be divided into the following three main categories in terms of ballast circuitry and their attempts on power-factor correction.

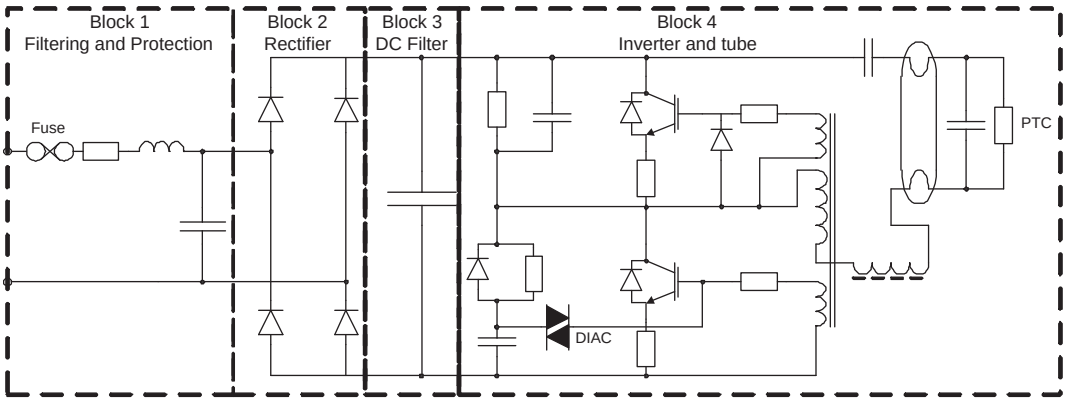

Figure 3.1 Typical CFL ballast circuit

LC tuned circuit

Passive filtering often uses inductor/capacitor combination with a desired resonance frequency (usually three times of the line frequency) placed before the rectifier. The advantage of this passive LC technique is its simplicity and ease of implementation. The 3^{rd} harmonic injection level is greatly reduced. However, the drawbacks are the physical size and weight for higher wattage CFL, which make it unattractive due to the limited space and inherent power loss. It is an ineffective way of harmonic filtering as the I_{THD} is usually between 90% and 120%.

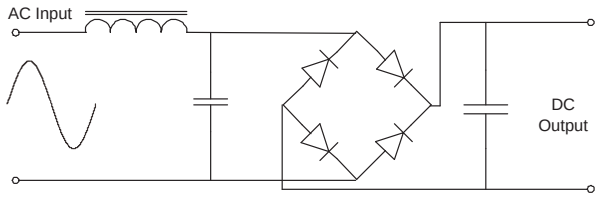

Figure 3.2 LC tuned circuit

Valley-Fill circuit

A better solution for reducing harmonics is by altering the CFL circuit to improve its current waveform. A Valley-Fill circuit, shown in Figure 3.3., splits the capacitor filter into two small values C_1 and C_2, which are alternatively charged and discharged using three diodes. However, this circuit results in a large DC voltage ripple, which produces lamp power and luminous flux fluctuation. As a result, it will reduce the lamp life. The improved Valley-Fill circuit shown in Figure 3.4 adds two identical capacitors of small value as a voltage doubler to extend the current conduction angle near the zero crossing. The resistor R_1 removes the charging current spikes at the voltage peak. This is a cost effective way of reducing harmonics as the I_{THD} can be significantly reduce to less than 40%.

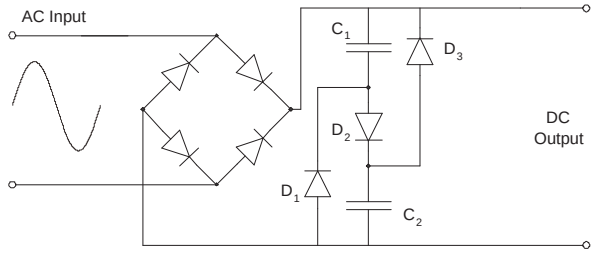

Figure 3.3 Valley-Fill filtering circuit

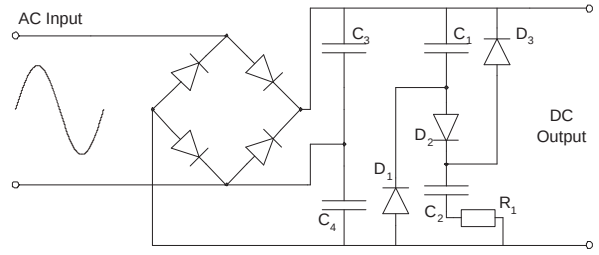

Figure 3.4 Improved Valley-Fill circuit

Active Power-Factor control

Active filtering is more advanced and costly method to achieve a high power-factor electronic ballast. High efficiency controlled switch is used to correct the input power-factor. Figure 3.5 shows an active boost converter which can be operated in discontinuous conduction mode with constant frequency and duty cycle to gain a power-factor close to unity. Dedicated IC chips are manufactured for controlling the switch in these active power-factor controlled ballasts. It has a total power-factor close to unity, but it is the most expensive one to manufacture. Typically, the I_{THD} is less than 10%.

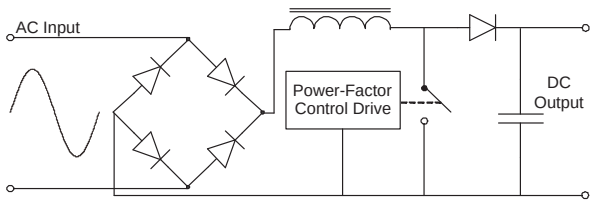

Figure 3.5 Active filtering circuit

3.2.3 CFL simulation model

The CFL harmonic performance varies greatly with the topology of its power-factor correction circuit. Therefore, there is a compromise between the generation of harmonics and cost, and often CFL life-time. Although the Standard AS/NZS 61000.3.2 provides the limitation on the harmonic current emission from the devices, it is not mandatory to follow this joint Australia and New Zealand standard. Due to the price competition, manufacturers have introduced the simplest ballast design with neither harmonic filter nor power-factor correction circuit. It usually has very high harmonic current levels, which depend on the size of the capacitor and front resistor, but is the cheapest to manufacture. The I_{THD} is normally from 110% up to 200%. Currently, there is an ongoing debate among the equipment manufacturers, electricity companies and also in standard setting bodies to draw the line regarding the acceptable power quality and hence the cost of CFL. In order to perform a detailed analysis of CFLs' external harmonic behaviour, a nominal rating of 20 Watts rectifier with capacitor filtering circuit, as shown in Figure 3.6, is used as a general CFL simulation model as this is the most common size. It has a I_{THD} of 110% at the base case.

3.3 CFL HARMONIC MODELLING

3.3.1 Harmonic perturbation analysis (HPA) on CFL

The purpose of harmonic perturbation analysis (HPA) on CFL is to find the harmonic interaction between CFL harmonic voltage and current around its operating point. The base case of HPA,

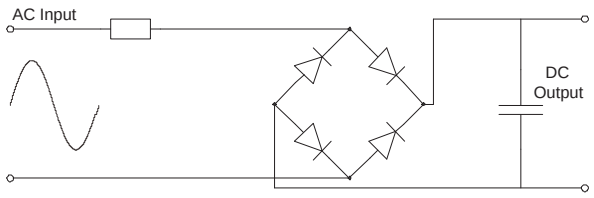

Figure 3.6 CFL simulation model

shown in Figure 3.7(a), assumes that the CFL is connected to an ideal voltage source, and its current waveform is decomposed into a series of harmonic components as the base case value I_{base}. The perturbation voltage $V_{perturbed}$, shown in Figure 3.7(b), is superimposed one frequency at a time to model the presence of voltage distortion of the supply voltage. Under each perturbation case, the harmonic current components $I_{perturbed}$ vary from their I_{base} by ΔI_h. The simulation is conducted in PSCAD/EMTDC environment using multiple run component to provide an variable voltage angle from 0 to 360 degrees with an step size of 10 degrees for each voltage perturbation. During this process, both the corresponding harmonic voltage and related current phasors are recorded as the angle of perturbed voltage changes. Then the data is imported into MATLAB to calculate and plot their resultant admittance locus using Equation 2.1. As a result, the frequency coupling admittance tensors can be found using Equation 2.9.

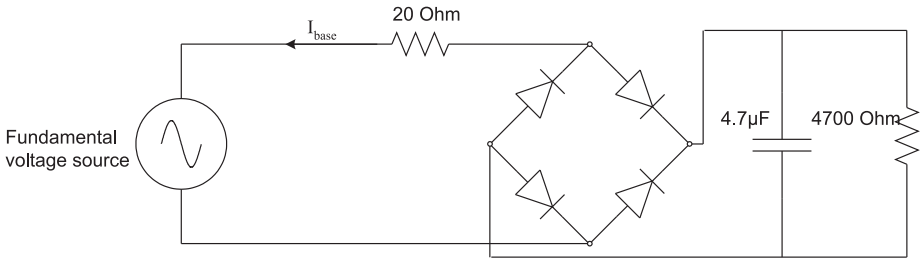

(a) Base case

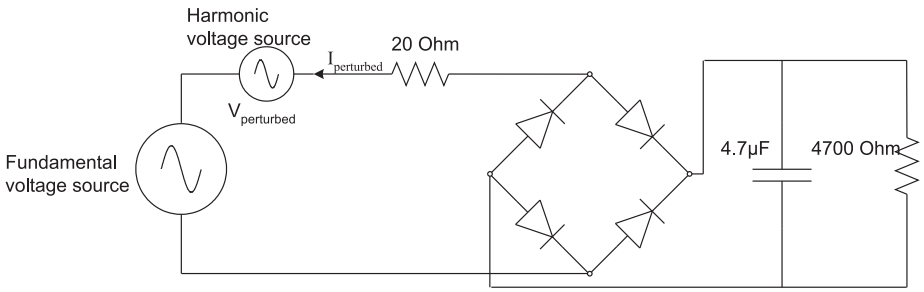

(b) Perturbation case

Figure 3.7 Harmonic perturbation analysis PSCAD/EMTDC simulation circuit

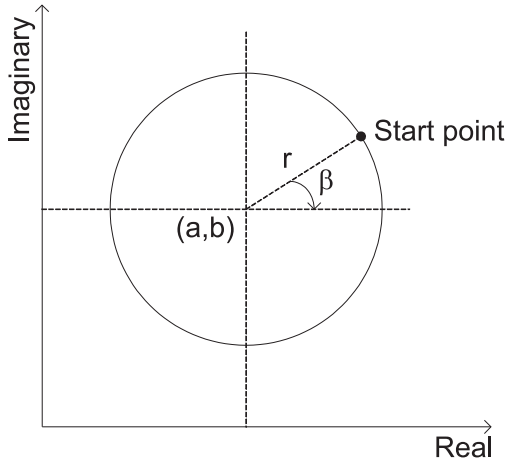

Figure 3.8 Complex admittances locus for a tensor admittance

Initially, the HPA is conducted at a voltage perturbation level of 0.1% of the fundamental voltage in a frequency range from the 1^{st} up to the 29^{th} for all odd harmonic orders as CFL current waveform does not contain any even harmonics. For example, by inserting a 5^{th} harmonic voltage source V_5, the coupling between the ΔI_h and V_5 yields their admittance terms $[\frac{\partial I_1}{\partial V_5}, \frac{\partial I_3}{\partial V_5}, \frac{\partial I_5}{\partial V_5}, \cdots, \frac{\partial I_m}{\partial V_5}, \cdots, \frac{\partial I_{29}}{\partial V_5}]^{-1}$, which are located in the same column of the CFL admittance tensor matrix. Each tensor describes the sensitivity of the m^{th} harmonic current components I_m to the variation of 5^{th} harmonic voltage V_5. If there is no dependency between the I_m and V_5, then the sensitivity tensor is zero. Otherwise, it should be represented as $\begin{bmatrix} Y_{11} & Y_{12} \\ Y_{21} & Y_{22} \end{bmatrix}$ where $Y_{11} \neq Y_{22}$ and $Y_{12} \neq -Y_{21}$ (See Appendix A). With all 15 perturbations, 225 ($= 15 \times 15$) admittance tensors have been calculated based on their double traced circle excluding $Y_{1,9}$ and $Y_{3,9}$, which have been found to not exhibit the phase dependency character. Then all these frequency coupling admittance matrices are combined into one matrix as Y_{CFL} with an overall dimension of 30×30.

Linearization of CFL at 0.1% voltage perturbation level provides its slope admittance under small voltage distortion around the fixed base case operating point. During the small perturbation process such as this, all the frequency coupling admittances rotate at their constant magnitudes with a double step size in the clockwise direction as the voltage angle changes from 0 to 2π. This circular locus has a radius r with a centre at (a, b) and ration β, which corresponds to the initial angle when applied voltage of phase 0 (See Figure 3.8). The relationship between the circle parameters and admittance tensor elements are as follow [23]:

$$a = \frac{1}{2}(Y_{11} + Y_{22}) \tag{3.2}$$

$$b = \frac{1}{2}(-Y_{12} + Y_{21}) \tag{3.3}$$

$$r = \frac{1}{2}\sqrt{(Y_{11} - Y_{22})^2 + (Y_{12} + Y_{21})^2} \tag{3.4}$$

$$\beta = \tan^{-1}(\frac{Y_{12} + Y_{21}}{Y_{22} - Y_{11}}) \tag{3.5}$$

3.3.2 Optimization of CFL admittance tensors

Modelling and analysis of the harmonic behaviour of CFLs in an electrical network is difficult due to the individual small power rating and their widespread deployment. In addition, the voltage quality is not exactly the same along the feeder, and is even different for the same location between daytime and night. Therefore, the primary purpose of this research is to find a general CFL admittance matrix which can be applied to a wide range of voltage distortions. Table 3.1 shows a typical supply voltage as CFLs will experience recorded in a residential premise. Therefore, different voltage perturbation levels at each odd harmonic order have been adopted with maximum magnitudes slightly higher than the values listed in Table 3.1. Figure 3.9(a) displays the loci of $Y_{3,5}$ as the angle of V_5 varies from 0 to 2π at the magnitudes of 0.1%, 1%, 2% and 3% of the fundamental voltage components respectively. It can be seen that their admittance loci are almost in the same phase dependent manner of two partially overlapped circles with similar magnitude.

The phase dependent admittance plot in Figure 3.9(a) also indicates that as the phase angle of V_5 changes from zero up to a certain angle θ, the locus starts to deviate from the original circle and travels in another circular path, and finally joins with the starting point. Figure 3.10 shows another example of locus $Y_{11,13}$ with a perturbation level of 0.92% of the fundamental voltage. Instead of having a double traced circle, the locus appears as partial overlapped circles with different centre points and radius, which is a typical locus for most of the cross-coupling admittance at higher voltage distortion, such as 11^{th} order and above. The large number of admittance plots have shown that the angle θ of V_n varies from case to case so that its coupling with ΔI_h cannot be categorized into two sets of fixed CFL admittance tensor matrix based on the voltage angle θ. Therefore, two types of optimization have been investigated: The first method is to average the tensor results based on the selected points, another approach is to average the admittance plot into one double traced circle and use Equation 3.2-3.4 to calculate the optimized tensor.

Averaging tensors

Since the admittance tensor corresponds to a circular admittance locus on the complex plane, the typical partial overlapped locus shown in Figure 3.9 (a) and Figure 3.10 can be fully described by three tensors. The first tensor characterizes how the phase changes when the voltage angle

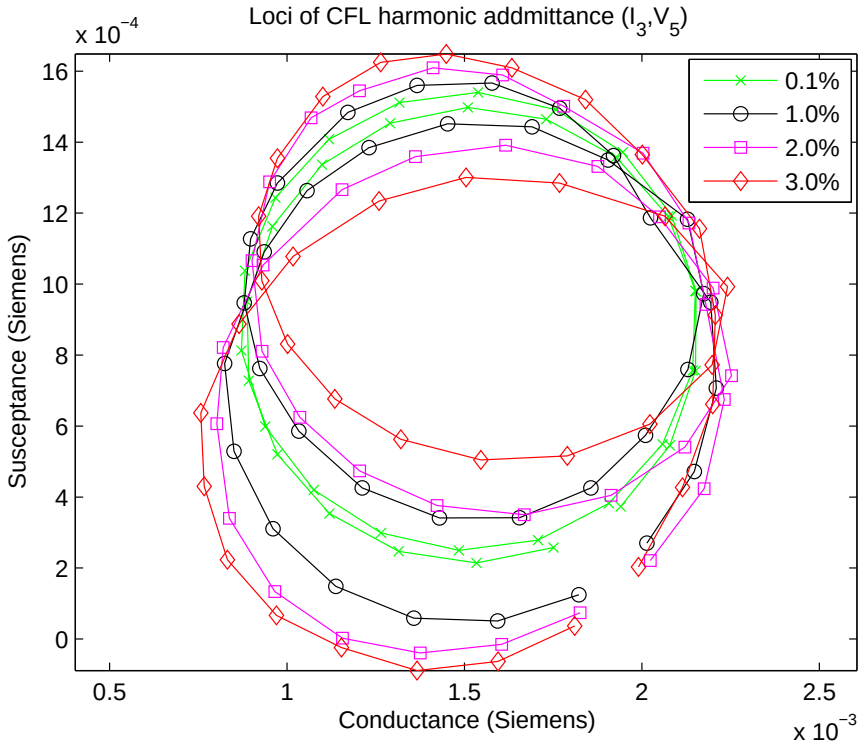

(a) Actual plot at different levels of perturbations

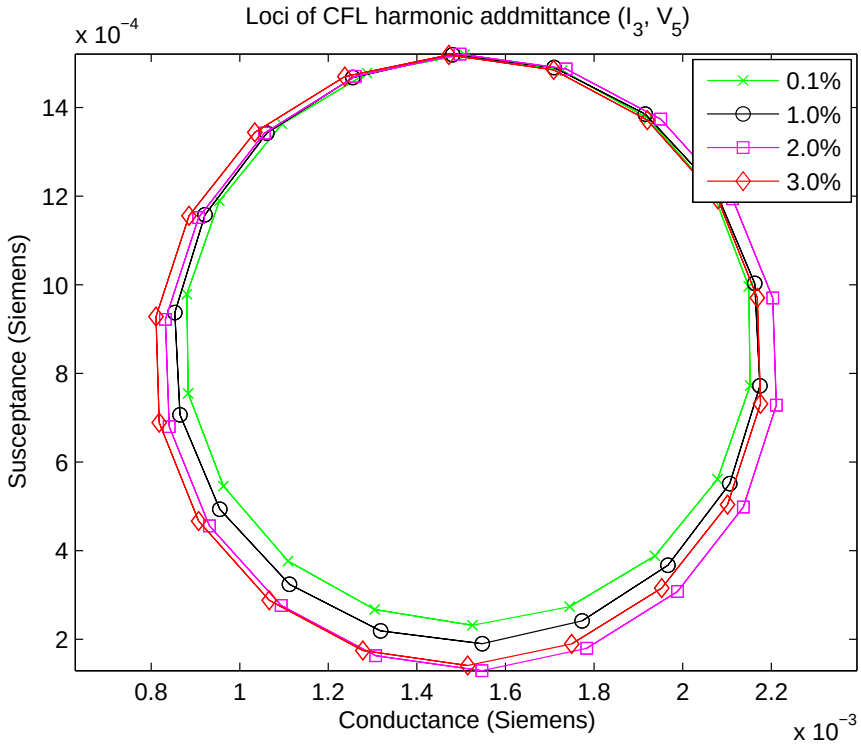

(b) Averaged plot at different levels of perturbations

Figure 3.9 Phase dependency plots of CFL admittance $Y_{3,5}$ at different harmonic voltage perturbations

Table 3.1 Supply voltage measured at service main

Harmonic Order	Frequency(Hz)	V_{RMS} (V)	$\%V_{RMS}$	$\angle\theta$(Degree)
1	50	234	99.9	0
2	100	0	0.0	-84
3	150	0.8	0.3	91
4	200	0	0.0	-34
5	250	6.8	2.9	-174
6	300	0	0.0	44
7	350	2.8	1.2	8
8	400	0	0.0	26
9	450	0.23	0.1	-179
10	500	0	0.0	9
11	550	0.46	0.2	-27
12	600	0	0.0	112
13	650	0.92	0.4	15
14	700	0	0.0	4
15	750	0.23	0.1	-156
16	800	0	0.0	-15
17	850	0.23	0.1	-18
18	900	0	0.0	161
19	950	0.23	0.1	49
20	1000	0	0.0	70
21	1050	0.46	0.2	-170
22	1100	0	0.0	6
23	1150	0.23	0.1	10
24	1200	0	0.0	169
25	1250	0.23	0.1	141
26	1300	0	0.0	23
27	1350	0.23	0.1	-167
28	1400	0	0.0	-165
29	1450	0.23	0.1	14

increases from zero up to angle θ, the second tensor describes the admittance locus as the voltage angle increases from θ to 360 degree. In addition, the start and end points in the locus are used to calculate the 3^{rd} tensor. As an illustration, Figure 3.10 shows how the arbitrarily chosen points have been selected to calculate the three tensors. The resulting three tensors are:

$$Y_{3,5_{1st}} = \begin{bmatrix} 1.82e-3 & -1.05e-3 \\ 0.003e-3 & 1.02e-3 \end{bmatrix} S \tag{3.6}$$

$$Y_{3,5_{2nd}} = \begin{bmatrix} 1.54e-3 & -1.81e-3 \\ 0.504e-3 & 1.61e-3 \end{bmatrix} S \tag{3.7}$$

$$Y_{3,5_{3rd}} = \begin{bmatrix} 1.81e-3 & -1.22e-3 \\ 0.037e-3 & 1.05e-3 \end{bmatrix} S \tag{3.8}$$

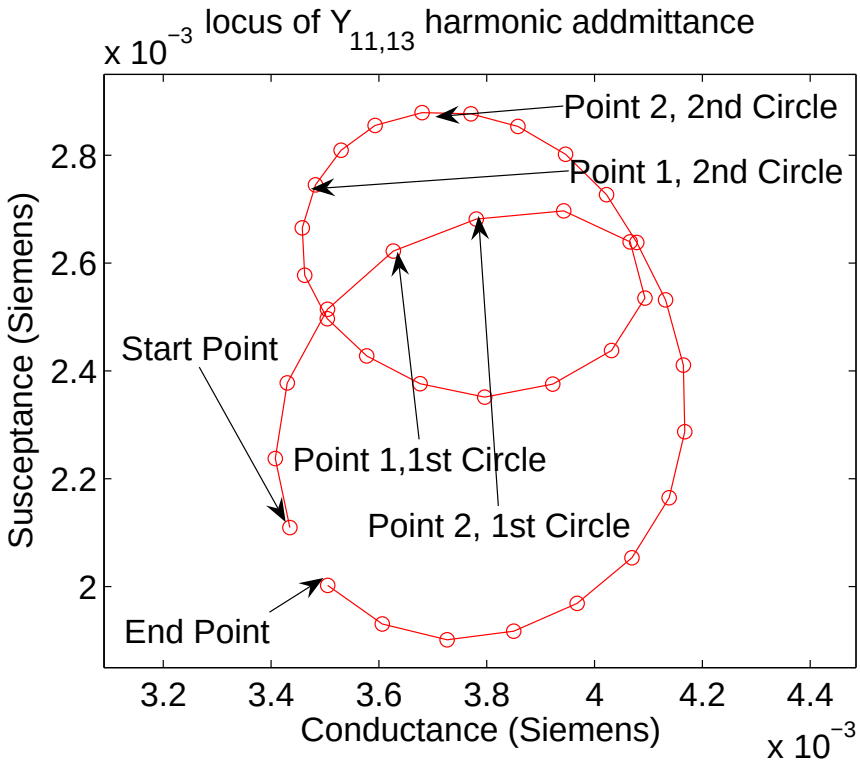

Figure 3.10 Locus of $Y_{11,13}$ at 0.92% voltage perturbation

The approximation of $Y_{3,5}$ is the average value of the three tensors:

$$Y_{3,5_{average}} = \begin{bmatrix} 1.72e-3 & -1.36e-3 \\ 0.18e-3 & 1.22e-3 \end{bmatrix} S \tag{3.9}$$

Similarly, Figure 3.11(a) shows another example of phase dependent CFL admittance $Y_{5,5}$ under 0.1%, 1%, 2% and 3% voltage distortion, the admittance tensors for 3% voltage distortion were calculated and are listed below:

$$Y_{5,5_{1st}} = \begin{bmatrix} 1.34e-3 & -2.45e-3 \\ 2.13e-3 & 0.47e-3 \end{bmatrix} S \tag{3.10}$$

$$Y_{5,5_{2nd}} = \begin{bmatrix} 1.01e-3 & -2.67e-3 \\ 2.50e-3 & 0.64e-3 \end{bmatrix} S \tag{3.11}$$

$$Y_{5,5_{3rd}} = \begin{bmatrix} 1.51e-3 & -2.07e-3 \\ 2.07e-3 & 0.39e-3 \end{bmatrix} S \tag{3.12}$$

The average value of $Y_{5,5}$ is thus:

$$Y_{5,5_{average}} = \begin{bmatrix} 1.28e-3 & -2.39e-3 \\ 2.23e-3 & 0.49e-3 \end{bmatrix} S \tag{3.13}$$

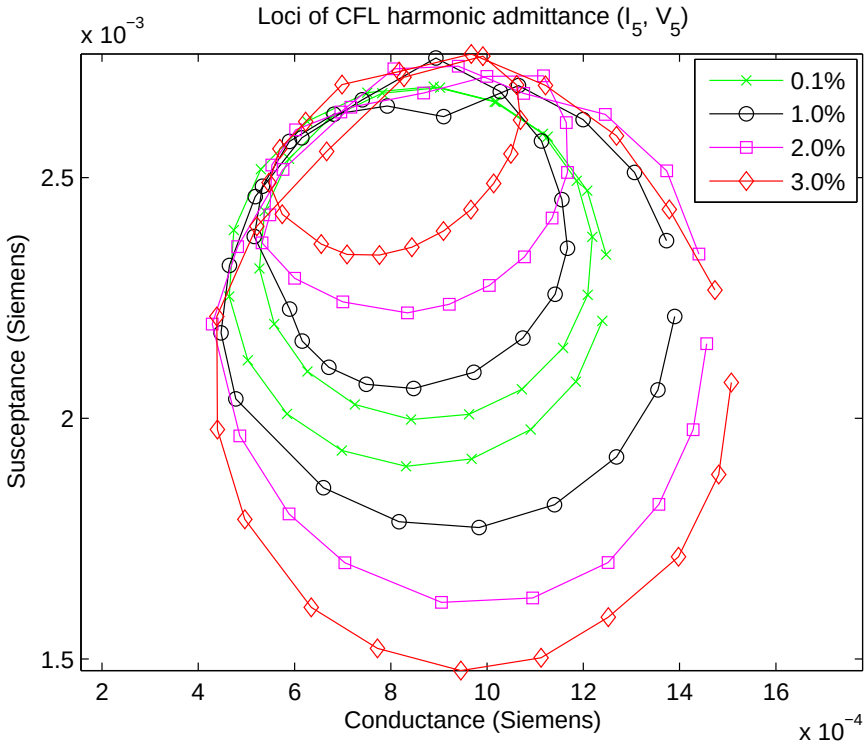

(a) Actual plot at different levels of perturbations

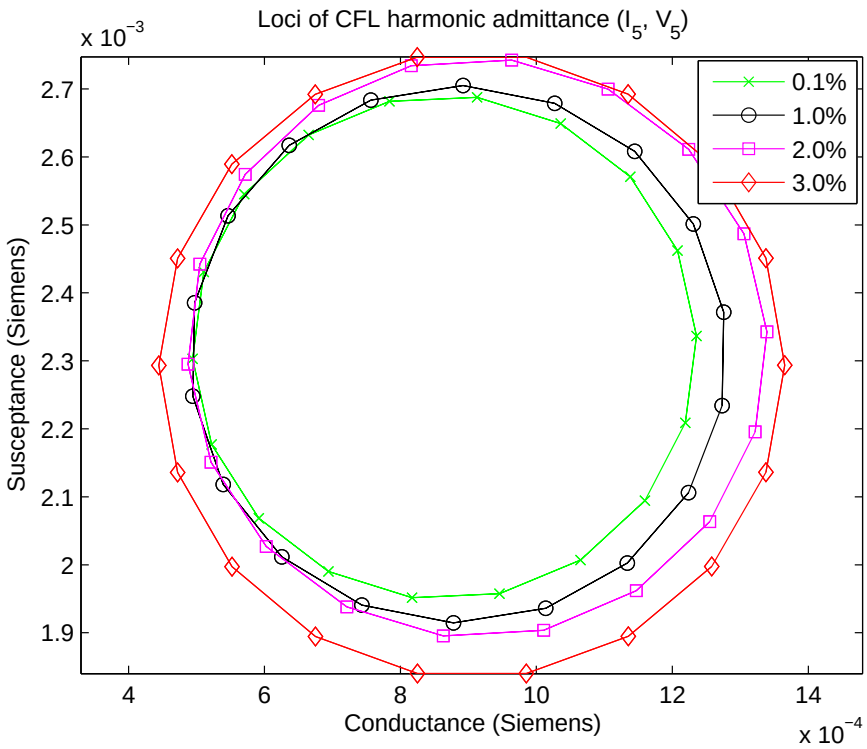

(b) Averaged plot at different levels of perturbations

Figure 3.11 Phase dependency plots of CFL admittance $Y_{5,5}$ at different harmonic voltage perturbations

Averaging the locus

Instead of averaging the tensor elements, an optimal solution can also be made by averaging all the admittances into one double traced circle as shown in Figure 3.9(b) and 3.11(b). By rearranging equations 3.2-3.5 in terms of the tensor elements, $\begin{bmatrix} Y_{11} & Y_{12} \\ Y_{21} & Y_{22} \end{bmatrix}$ can be solved using Equations 3.14-3.21 below:

$$\text{if } -\tfrac{\pi}{2} < \beta < \tfrac{\pi}{2}$$

$$Y_{11} = \frac{r}{\sec(\beta)} + a \tag{3.14}$$

$$Y_{22} = -\frac{r}{\sec(\beta)} + a \tag{3.15}$$

$$\text{elsewhere}$$

$$Y_{11} = -\frac{r}{\sec(\beta)} + a \tag{3.16}$$

$$Y_{22} = \frac{r}{\sec(\beta)} + a \tag{3.17}$$

$$\text{if } 0 < \beta < \pi$$

$$Y_{12} = \frac{r \times \tan(\beta)}{\sec(\beta)} - b \tag{3.18}$$

$$Y_{21} = \frac{r \times \tan(\beta)}{\sec(\beta)} + b \tag{3.19}$$

$$\text{elsewhere}$$

$$Y_{12} = -\frac{r \times \tan(\beta)}{\sec(\beta)} - b \tag{3.20}$$

$$Y_{21} = -\frac{r \times \tan(\beta)}{\sec(\beta)} + b \tag{3.21}$$

where $\beta \neq \pm\frac{\pi}{2}$ (See Appendix B). The approximation of the admittance tensors $Y_{3,5}$ and $Y_{5,5}$ for a voltage distortion around 3% voltage distortion are shown in Equation 3.22 and 3.23:

$$Y_{3,5_{approxmation}} = \begin{bmatrix} 1.75e-3 & -1.47e-3 \\ 0.19e-3 & 1.24e-3 \end{bmatrix} S \tag{3.22}$$

$$Y_{5,5_{approximation}} = \begin{bmatrix} 1.34e-3 & -2.45e-3 \\ 2.14e-3 & 0.47e-3 \end{bmatrix} S \tag{3.23}$$

By comparing $Y_{3,5_{average}}$ with $Y_{3,5_{approximation}}$ and $Y_{5,5_{average}}$ with $Y_{5,5_{approximation}}$, both optimization approaches show great similarity. However, the approach of averaging the locus and finding the related tensor is more computational efficiency. Therefore, all the 225 cross-coupling admittance tensors are calculated using this method and combined together as the fixed Y_{CFL} to form a general Norton equivalent circuit for the CFL. Figure 3.12 shows the structure and magnitude of this overall admittance tensor matrix. As it can be that the magnitude of the admittance tensor increases with the order of harmonic frequency. The diagonal terms have the strongest

coupling, followed by the coupling between n^{th} order and $(n\pm2)^{th}$ order at its off-diagonal terms. Hence, the matrix is dominated by a tri-diagonal structure.

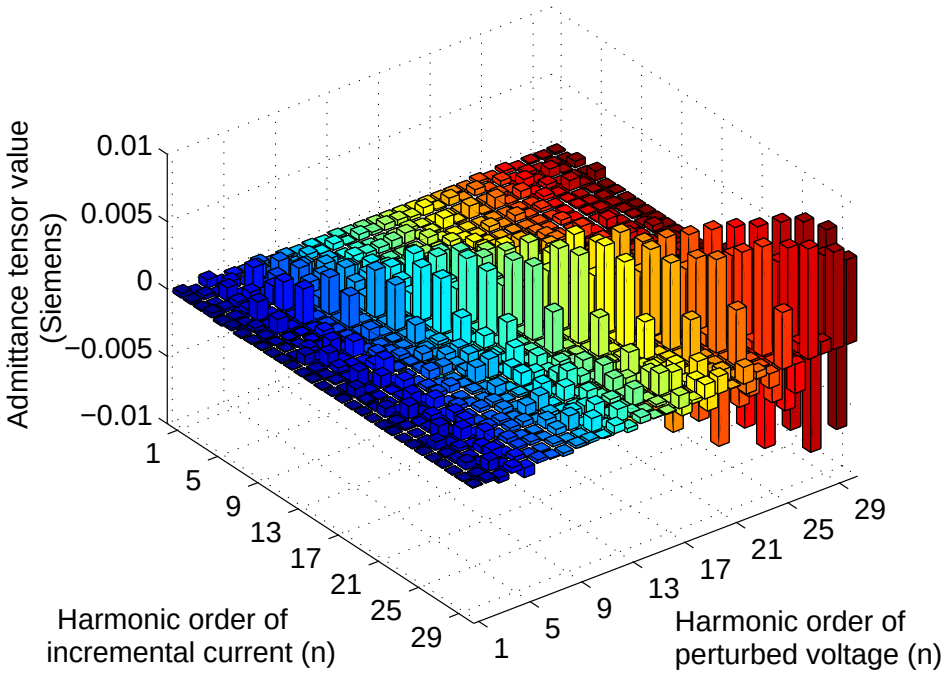

Figure 3.12 CFL admittance tensor matrix

3.3.3 CFL Norton equivalent validation

This proposed Norton equivalent model for the CFL is applied to a single phase LV network with a typical V_{THD} of 3.26% at the supply terminal. Three residential loads shown in Figure 3.13(a) are included with five CFLs per house. The five CFLs are lumped into one Norton equivalent, and the remaining house load is represented by a RL parallel circuit as shown in Figure 3.13(b). The overall nodal system admittance matrix Y_{system} is shown in Equation 3.24. Each off-diagonal element $Y_{k,l}$ is the negative sum of the branch admittance between node k and node l, and diagonal element $Y_{k,k}$ includes the admittance of the branches which terminate on node k, including node k to the ground. They are usually represented as either zero or complex numbers, which are then converted into 2×2 matrices as $Y = \begin{bmatrix} Y_R & -Y_I \\ Y_I & Y_R \end{bmatrix}$ to allow incorporation with the CFL admittance tensors. The overall structure of the full coupled system admittance matrix is shown in Figure 3.14[1].

[1]The notch on the diagonal of the system admittance matrix represents the weak frequency coupling of admittances $Y_{1,9}$, and $Y_{3,9}$.

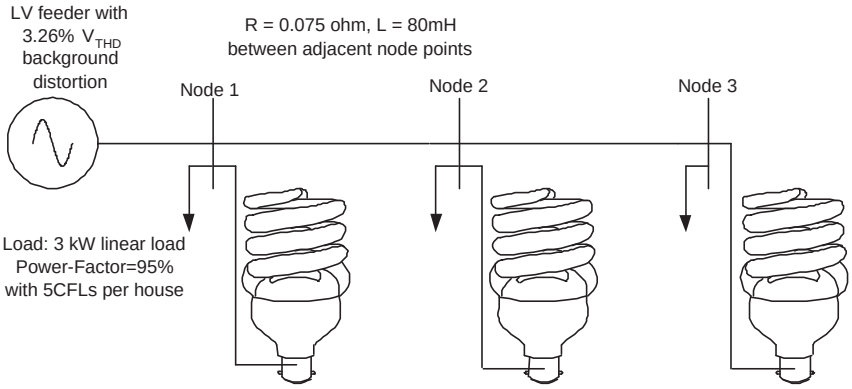

(a) Time domain simulation model

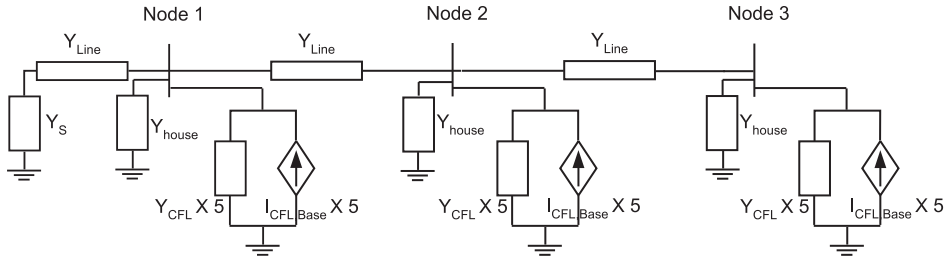

(b) Equivalent frequency domain simulation model

Figure 3.13 Test model

$$Y_{system} = \begin{bmatrix} Y_{1,1} & Y_{1,2} & Y_{1,3} \\ Y_{2,1} & Y_{2,2} & Y_{2,3} \\ Y_{3,1} & Y_{3,2} & Y_{3,3} \end{bmatrix} \tag{3.24}$$

The CFLs' harmonic current components at each node point are calculated in MATLAB using Equation 2.11-2.13. In order to validate the accuracy of the CFL Norton equivalent model, a detailed time domain simulation using PSCAD/EMTDC was performed as a benchmark. The solution uses a 50 μs time-step with a simulation length of 1s. All the spectra are derived from the final 0.02s of data using an FFT. The comparison results are shown in Figure 3.15-3.17 respectively. As evident from the comparison, most of the harmonic components show very good agreement. However, some errors have occurred at higher harmonic frequencies. This is mainly due to the high sensitivity of the admittance growth as the ΔI_h increases, which also correlates to the experimental observation [7, 28].

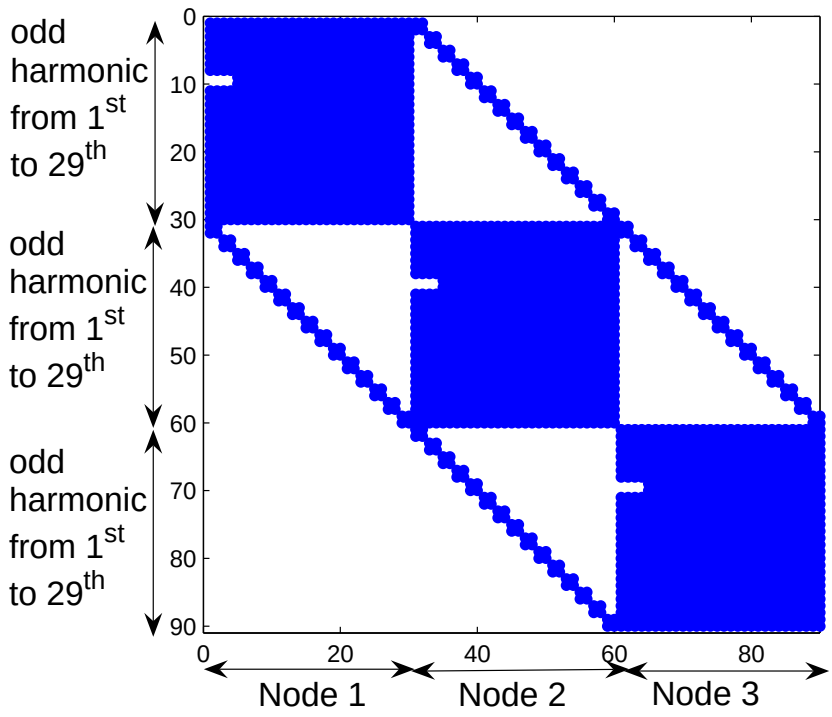

Figure 3.14 Harmonic domain system admittance matrix of the test model

3.4 CONCLUSIONS

This chapter has looked at the power-factor correction and harmonic performance of CFLs, and linked these to a general CFL simulation model. The harmonic perturbation analysis was conducted with a V_{THD} of 3.26%. Two approaches on the admittance tensor optimization have been adopted, and both methods have shown strong agreements. The developed CFL Norton equivalent model has shown good comparison with the time domain simulation, and is also suitable for a general CFL harmonic analysis model with non-sinusoidal supply voltage.

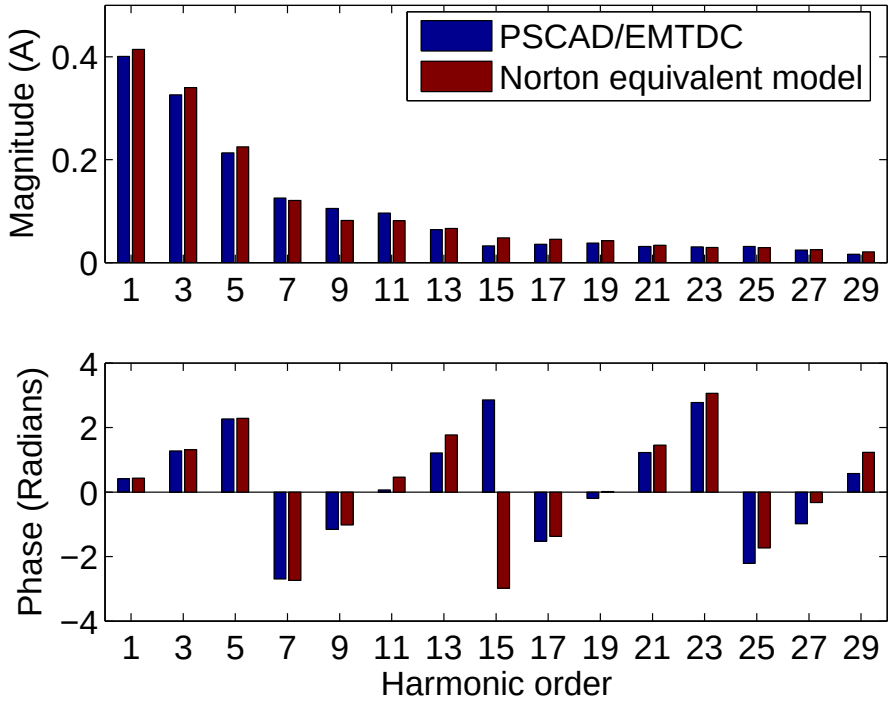

Figure 3.15 CFLs harmonic current injection at node 1

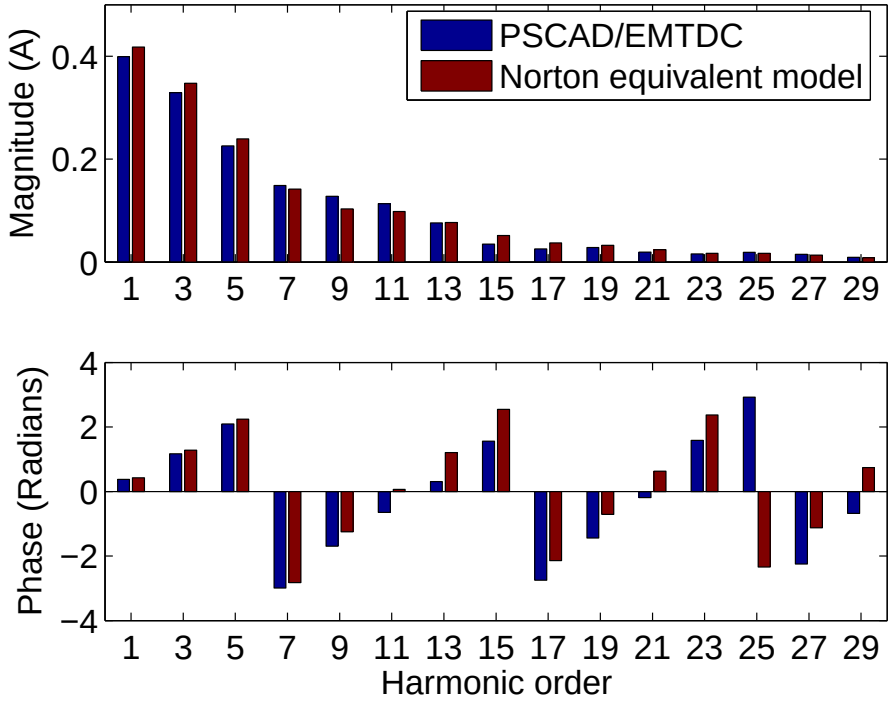

Figure 3.16 CFLs harmonic current injection at node 2

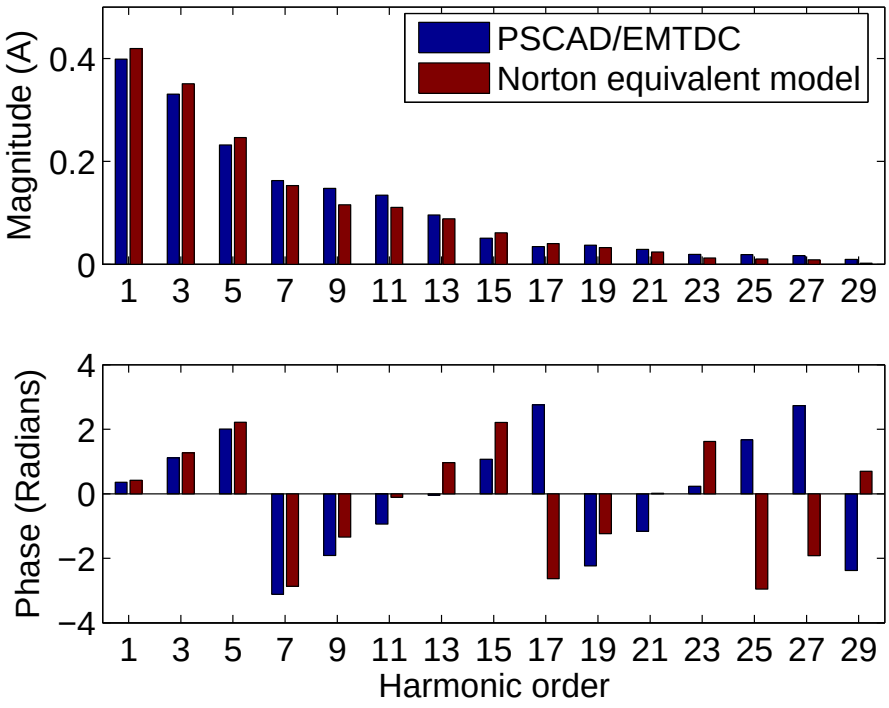

Figure 3.17 CFLs harmonic current injection at node 3

Chapter 4

CASE STUDY: HARMONIC ASSESSMENT OF WIDESPREAD USE OF CFLs IN A DISTRIBUTION SYSTEM

4.1 INTRODUCTION

The growing deployment of CFLs in residential and commercial premises has raised the electricity utilities' concern over power quality on their medium and low voltage feeders. Although the input power of a single CFL is insignificant with an average rating of 20 Watts, 30,000 residential customers using a few CFLs per house are able to create a total load of 3 MW, which could be sufficient to cause unacceptable V_{THD} along the feeders. CFLs are generally characterized by their harmonic emission levels, as their current waveform drawn vary greatly with their circuit design. A variation of 5% to 200% in I_{THD} has been noticed from the lab.

In order to translate these injected harmonic current into the supply terminal voltage distortion, the structure of the distribution network must be known. One of the early work [27] has shown that no more than 1% of the total loading was allowable for CFLs in order to maintain the 5% V_{THD} limits on a 15 kV, 10 MVA feeder. Another investigation [18] has also found that replacing 30% of the incandescent lamps by CFLs would result some LV feeder exceeding the regulator 8% V_{THD} threshold.

For a particular distribution network, the maximum tolerable level of CFLs is dependent on both the topology of the CFL circuit, and system background voltage distortion (partly caused by other nonlinear loads connected to the feeders and also the system strength). Recently, a study [28] has also been applied to a typical New Zealand distribution system by assuming five CFLs per house. The investigation was performed using different classes of CFLs in the network, and the resultant V_{THD} varied from 0.75% to 3.5% on the LV feeders. However, this work used fixed harmonic current source approach, which is usually not the case when many CFLs are connected to the network. This chapter extends this harmonic assessment by using CFL Norton equivalent representation developed in the previous chapter to provide an improved harmonic analysis.

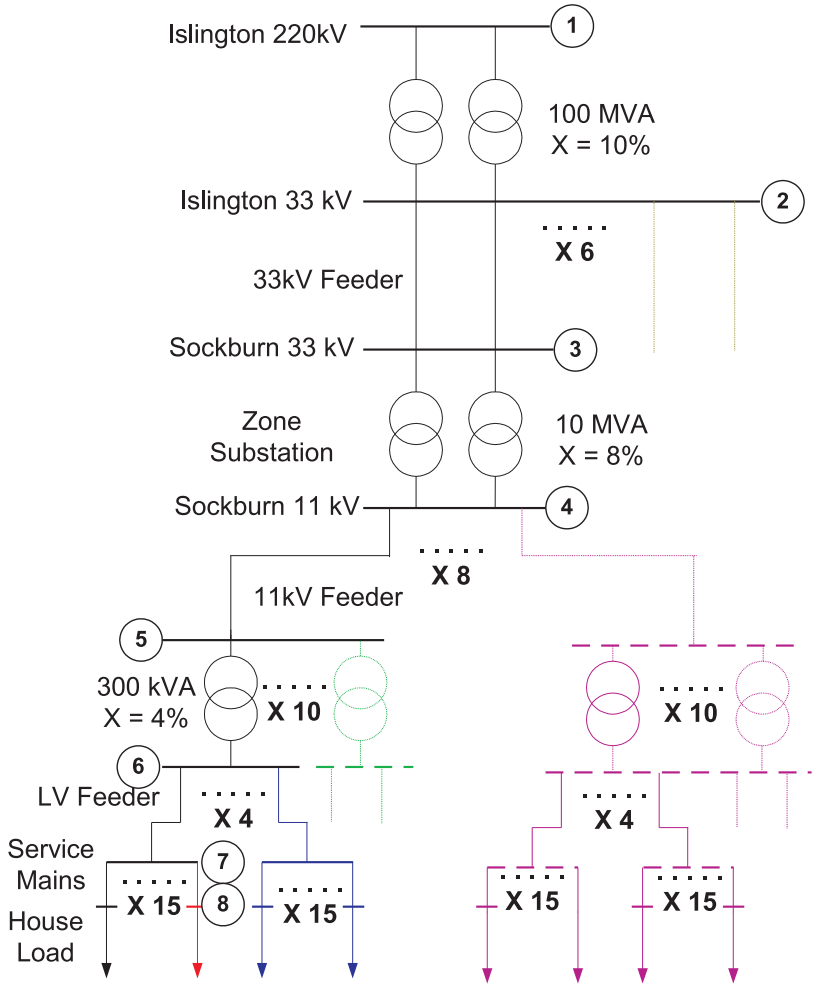

Figure 4.1 Distribution system layout

4.2 DISTRIBUTION SYSTEM MODELLING

Distribution companies in New Zealand are responsible for delivering the electricity from the GXP (Grid eXit Point) to the local customers. Figure 4.1 illustrates a typical layout of the urban distribution network. It has 15 residential loads along each LV feeder, and every 4 LV feeders are supplied by one 300 kVA distribution transformer, then 10 of these transformers are connected to a 11 kV feeder, 8 of these 11 kV feeders are supplied from one zone substation, and finally 6 zone substations are connected to the 33 kV busbar at the GXP. As the residential loads are assumed to be equally distributed between the three phases, a single-phase analysis approach is used. The high voltage transmission lines are modelled using lumped circuit π model, and the short distance of LV feeders are modelled as series impedances. By neglecting the magnetizing current and no load losses, a RL series circuit is used to present the internal impedance of the power transformer. Each residential customer is assumed to have a 3 kW linear load with a power-factor of 95%, and is represented by a parallel RL equivalent circuit. The 5 CFLs per

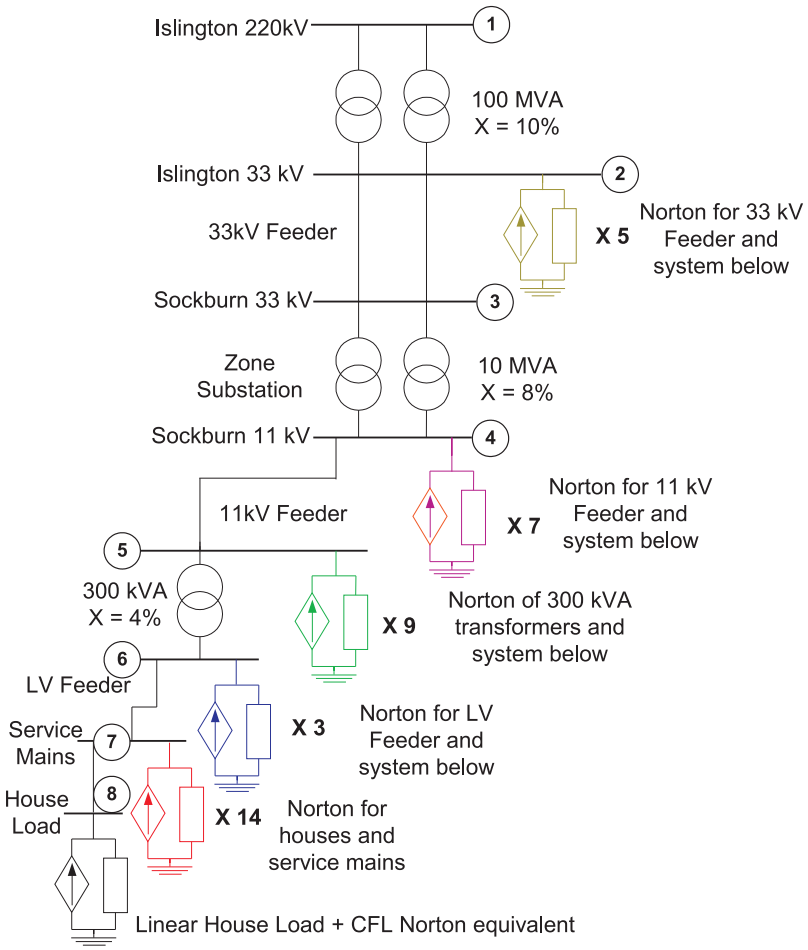

Figure 4.2 Simulation model

house are lumped as one Norton equivalent, then added to its residential load model to develop an overall Norton equivalent for each house. Every 15 houses are modelled at the end of each LV feeder. All the resistive components in the network are assumed constant at all frequencies, and the reactance is calculated by taking the 50 Hz inductance value and multiplying by the corresponding harmonic order. One branch of the distribution system is detailed while the effects of all other feeders and upper stream are represented by their Norton equivalents, as shown in Figure 4.2.

4.3 SIMULATION RESULTS

4.3.1 Harmonic current injection on V_{THD}

The mathematical model based on Figure 4.2 forms a set of linear equations as shown in Equation 4.1. Both overhead transmission lines (OHL) and underground cables (UGC) parameters are used separately for the harmonic studies to represent a predominant OHL distribution system and a predominate UGC distribution system. As most of the distribution network is a

mixture of overhead lines and underground cables, these two sets of simulation would provide a reasonable boundary for the actual system. Figure 4.3 displays the overall structure of the system admittance matrix in the harmonic domain, which is similar to Figure 3.14. Due to the star-delta winding configuration of the distribution transformer, there is no triplen harmonic current penetrating through to the upstream network.

$$\begin{bmatrix} 0 \\ 5 \times I_{Norton_{33kVFeeder}} \\ 0 \\ 7 \times I_{Norton_{11kVFeeder}} \\ 9 \times I_{Norton_{Xfr33kVA}} \\ 3 \times I_{Norton_{LVFeeder}} \\ 14 \times I_{Norton_{HouseMains}} \\ I_{Norton_{House}} \end{bmatrix} = \begin{bmatrix} Y_{11} & Y_{12} & Y_{13} & Y_{14} & Y_{15} & Y_{16} & Y_{17} & Y_{18} \\ Y_{21} & Y_{22} & Y_{23} & Y_{24} & Y_{25} & Y_{26} & Y_{27} & Y_{28} \\ Y_{31} & Y_{32} & Y_{33} & Y_{34} & Y_{35} & Y_{36} & Y_{37} & Y_{38} \\ Y_{41} & Y_{42} & Y_{43} & Y_{44} & Y_{45} & Y_{46} & Y_{47} & Y_{48} \\ Y_{51} & Y_{52} & Y_{53} & Y_{54} & Y_{55} & Y_{56} & Y_{57} & Y_{58} \\ Y_{61} & Y_{62} & Y_{63} & Y_{64} & Y_{65} & Y_{66} & Y_{67} & Y_{68} \\ Y_{71} & Y_{72} & Y_{73} & Y_{74} & Y_{75} & Y_{76} & Y_{77} & Y_{78} \\ Y_{81} & Y_{82} & Y_{83} & Y_{84} & Y_{85} & Y_{86} & Y_{87} & Y_{88} \end{bmatrix} \begin{bmatrix} \Delta V_1 \\ \Delta V_2 \\ \Delta V_3 \\ \Delta V_4 \\ \Delta V_5 \\ \Delta V_6 \\ \Delta V_7 \\ \Delta V_8 \end{bmatrix} \quad (4.1)$$

According to Equation 2.14, the variation of the voltage distortion is subject to both the incremental voltage distortion caused by CFLs and the system background voltage distortion. These incremental harmonic voltages calculated from Equation 4.1 using both fixed harmonic current source and Norton equivalent are compared. Figures 4.4-4.7 show the details at 220 kV, 33 kV, 11 kV and 0.4 kV busbars respectively. From these plots, it can be seen that the harmonic voltage distortion at the 220 kV and 33 kV busbars are much smaller compared to that at the 11 kV and 0.4 kV busbars. Also the harmonic components at 11^{th} order and beyond decrease dramatically by considering CFLs' phase dependent admittance into the calculation. This also reflects that the CFLs harmonic injection at higher frequencies are more voltage dependent than at lower orders. Figure 4.8 also plots the incremental voltage distortion in terms of V_{THD} at each busbar of the distribution network. The graph shows that the major harmonic voltage distortion occurs at the LV feeder, and the maximum V_{THD} appears to be 1.47% for an overhead lines system and 1.22% for an underground cable system respectively. The CFL characteristic used for this simulation are listed in the 1^{st} column of Table 4.1, which is equivalent to the average CFL in the paper [28]. This is approximately 17% less than calculated by using fixed harmonic current source for both cases. As a result, Figure 4.9 displays the harmonic components of the background voltage distortion $V_{harbase}$ (listed in Table 3.1), incremental voltage distortion ΔV_{node} (caused by CFLs), and overall voltage distortion (vector sum of the $V_{harbase}$ and ΔV_{node}) respectively. As it can be seen that the overall voltage distortion tends to increase at most of the harmonic frequencies. Although this simulation has not included other types of nonlinear loads, this value would be a closer estimation to the "worst case" scenario with the widespread use of the average types of CFLs on the 0.4 kV busbars.

Due to the variation in CFL circuit topology, the current waveform drawn can be very different. For example, two 20 Watts CFLs of both Philips and Ecobulb brands would have significantly different impact on the harmonic levels, as shown in the 2^{nd} and 3^{rd} columns of Table 4.1. In

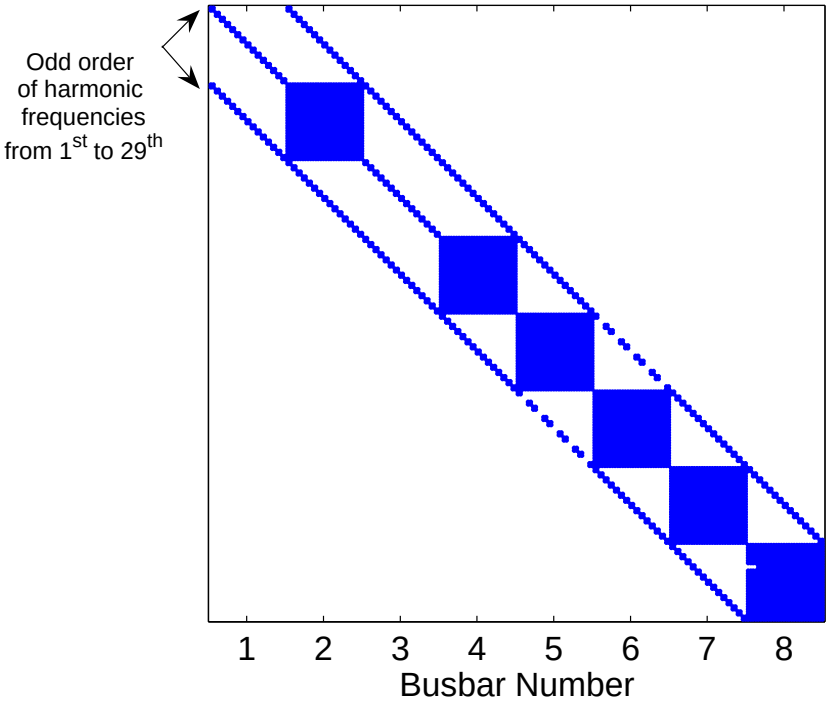

Figure 4.3 Harmonic domain distribution system admittance matrix

order to make sure their detrimental effects do not degrade the power quality of the supply, there is a debate on whether to regulate the harmonic current emissions for all harmonic frequencies or primarily focus on the 3^{rd} and 5^{th} harmonic components. This leads to the following two harmonic limitation criteria. The first criteria is to look at the harmonic current injection by mA/Watt for all harmonic frequencies. For a 20 Watts CFL, the maximum allowable harmonic levels using this approach are listed in Table 4.1 S(I) column. The second criteria is to limit the harmonic emission mainly for the 3^{rd} and 5^{th} harmonic components as a percentage of fundamental component (86% for the 3^{rd} harmonic and 61% for the 5^{th} harmonic). The spectra of a CFL model satisfy this criteria is given in Table 4.1 S(II) column.

The overall harmonic voltage distortion caused by these CFL models were also performed using Equation 4.1 with the background voltage distortion. Their results in terms of V_{THD} were calculated and are listed in the last row of Table 4.1. As it can be seen that the higher I_{THD} usually results in a higher harmonic voltage distortion. The CFL S(II) model leads to an extremely high harmonic voltage distortion. This is because although the 3^{rd} and 5^{th} harmonics are within the emission limits, the current waveform could still be a distinctive pulse at every half period. Often this type of CFLs seems to be more "energy efficient" due to its low real power drawn. However, it could cause a noticeable contribution to the voltage distortion of the supply. Moreover, its harmonic components at higher frequencies may also cause interference with other equipment.

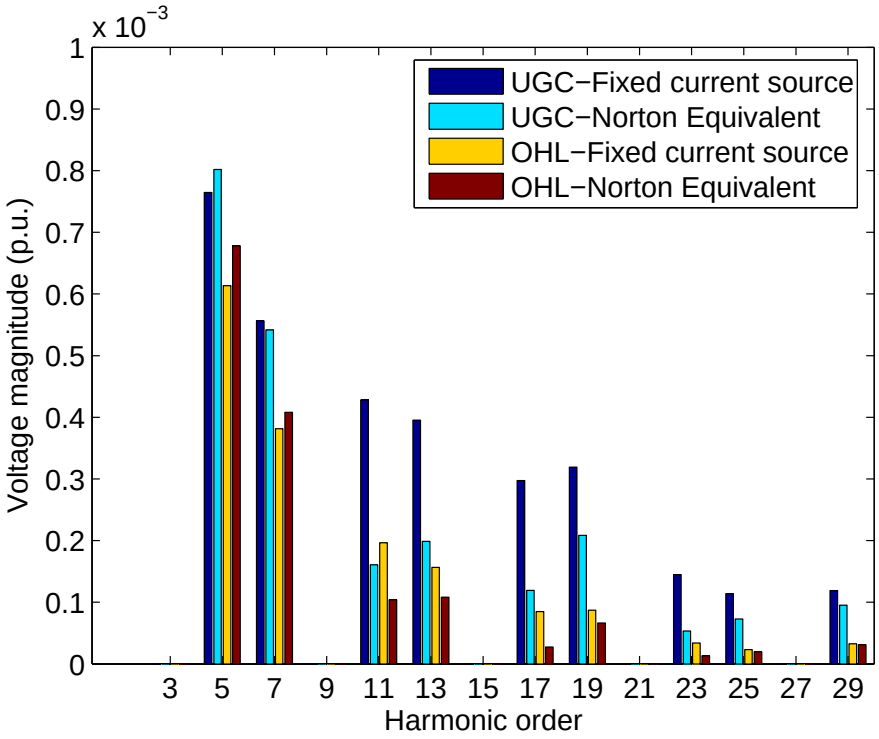

Figure 4.4 Incremental voltage distortion at 220 kV busbar

4.3.2 Harmonic interference with ripple control system

Ripple control system is widely used by New Zealand distribution companies as a load management tool to achieve an optimum use of their electrical network. For examples, switching hot water cylinders off during peak hours, controlling the street lighting and metering. It also plays a crucial role for these authorities to keep a reliable and secure supply to their customers without bringing any unnecessary capital investment and maintenance cost to their network.

The power system is used as the conducting medium for carrying the control signal from the transmitter located in the zone substation to numerous ripple relays which are directly connected to the targeted apparatus in the medium and low voltage networks. The transmitter generates the sinewave analogue signal pulses that replicate the control code as a modulated carrier with a magnitude between 2% and 5% of the nominal supply voltage. Amplification and attenuation of the ripple signal can happen due to the closeness between the network resonance frequency and its signaling frequency. These have occurred in the past due to the high voltage line parameters or power-factor correction capacitor with the internal impedance of the distribution transformer (low ripple frequency impedance seen from the ripple injector) [29, 30]. Depending on the local practice, the ripple control systems are designed with a frequency between 110 Hz and 1050 Hz. After propagating through the power network, the relays pick up the signal and demodulate into the control code to turn ON or OFF the loads. To avoid harmonic interference, the relays

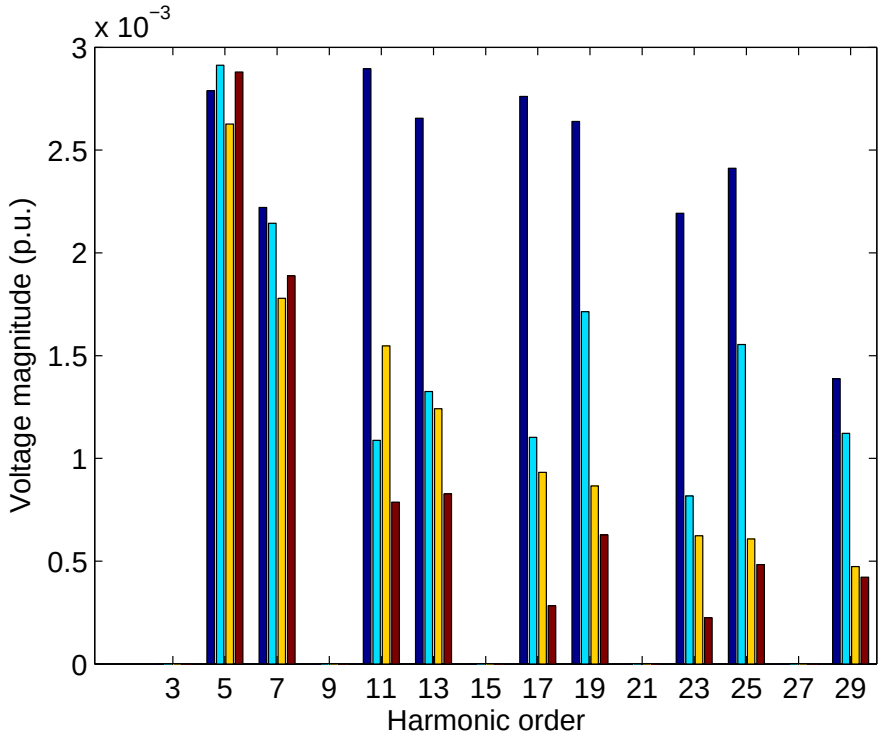

Figure 4.5 Incremental voltage distortion at 33 kV busbar

are designed and tested to ignore signals below certain threshold such as 0.3% of the nominal voltage.

Most modern ripple control systems are using inter-harmonic frequencies below 300 Hz as a signaling frequency to avoid the possible harmonic interference and resonance problems caused by the characteristics of the distribution network. However, some old ripple control systems still use 1050 Hz as a carrier frequency. Therefore, the 21^{st} harmonic voltage at the low voltage terminal has drawn the special attention. Figure 4.10 shows how the 21^{st} harmonic voltage components could be affected by all five different models of CFLs listed in Table 4.1 for both underground cables (Scenario 1) and overhead lines (Scenario 2) at the ripple signal receiving end (Service main), against the background voltage distortion when none of these CFL models is applied. Due to the small level of the 21^{st} harmonic current injection and phase angle difference between the resulted voltage distortion caused by CFLs and the background voltage distortion, the first four types of CFL models showed very limited impact to the overall V_{21}. However, the S(II) model results a large increment because of its high I_{21} injection. This also increases the possibility of the harmonic interference with the relays especially when the system loading is "light" at night.

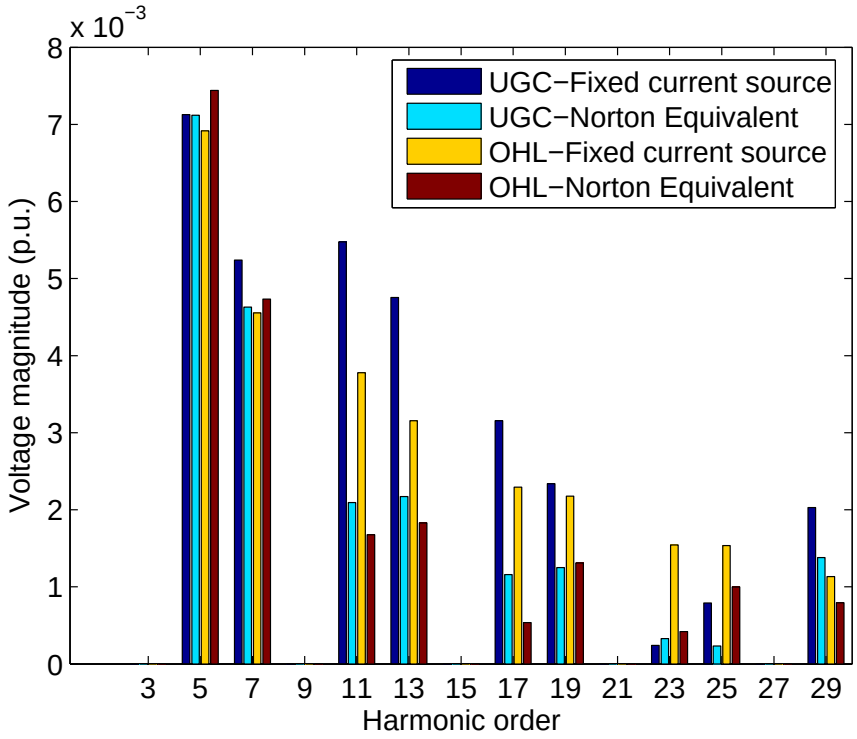

Figure 4.6 Incremental voltage distortion at 11 kV busbar

4.4 CONCLUSIONS

The effect of different types of CFL on a typical residential distribution network, assuming 5 CFLs per house, has been investigated. The simulation results show that the widespread use of CFLs have no major influences on the high and medium voltage systems, but could cause significant increase of voltage distortion to the low voltage feeders. Possible harmonic interference with old ripple control signal might occur, especially when system is lightly loaded. The feasible method of avoiding these issues is to ensure that the CFL is designed and manufactured in compliance with the appropriate emission limits. Although the S(II) model seems to be a very "energy-efficient" choice for customers, the large harmonic current injection is unacceptable. Therefore, the mA/Watt approach is more likely to be the solution between the CFL harmonic current emission and true energy-efficiency within a reasonable CFL price.

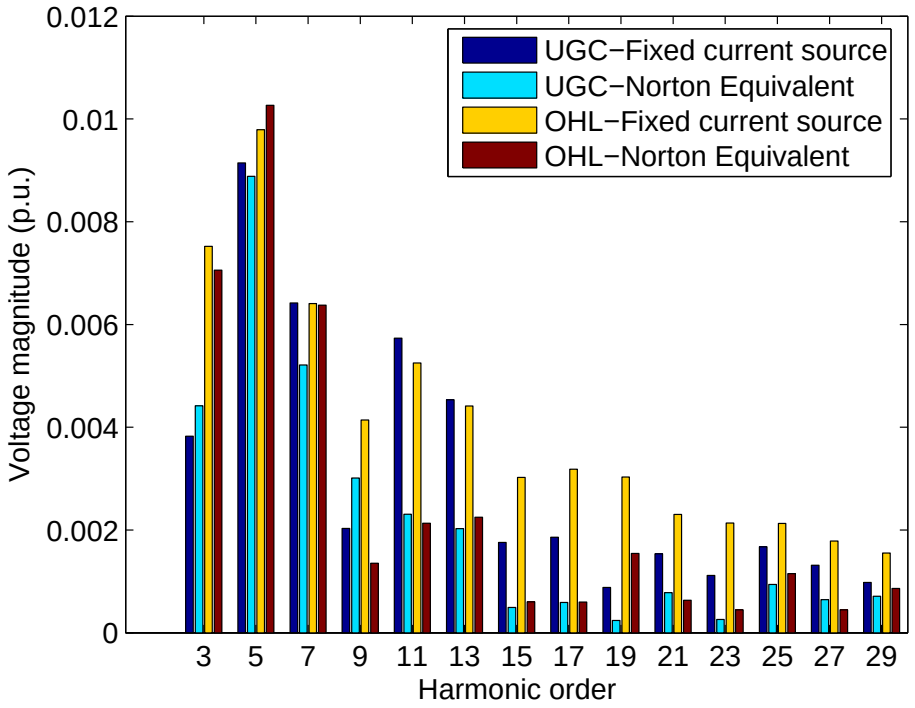

Figure 4.7 Incremental voltage distortion at 0.4 kV busbar

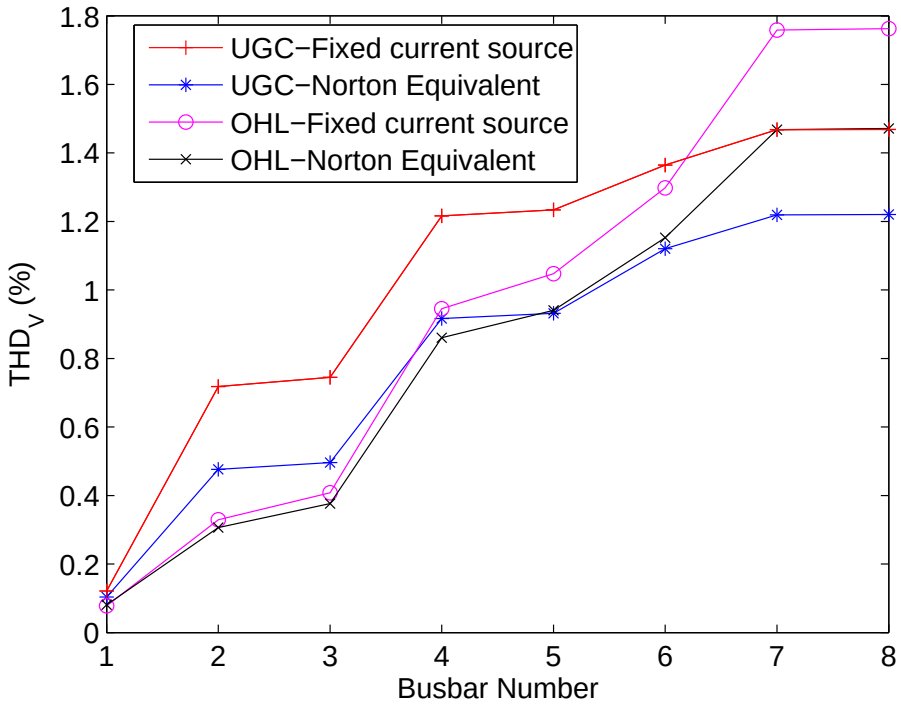

Figure 4.8 Incremental V_{THD} at each busbar caused by average CFLs [28]

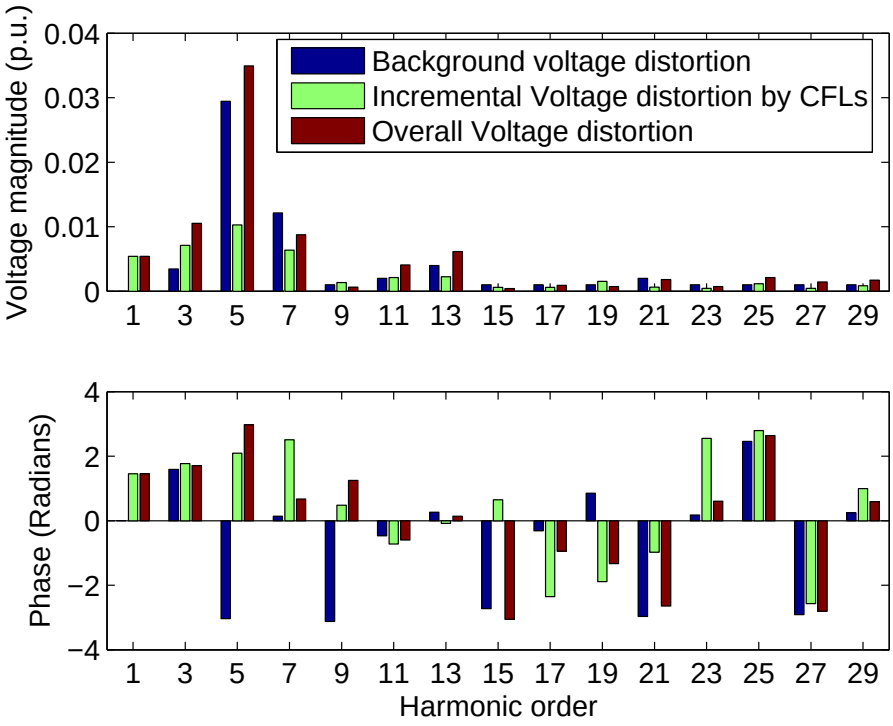

Figure 4.9 Harmonic voltage components at service main

Table 4.1 Harmonic current components of different CFL models and their effects on ΔV_{THD} to the supply

$mA\angle degree$	CFL simulation Model	Philips	EcoBulb	S(I)	S(II)
I_1	$82.9\angle 24.5$	$82.5\angle 32$	$85.0\angle 18$	$87\angle 20$	$88.2\angle 27$
I_3	$68.0\angle 75.1$	$71.3\angle -107$	$10.0\angle -151$	$68\angle 33$	$75.6\angle -127$
I_5	$45.0\angle 131$	$49.7\angle 124$	$22.0\angle 21$	$38\angle 62$	$53.4\angle 87$
I_7	$24.1\angle -157$	$28.3\angle 7$	$11\angle -128$	$20\angle -110$	$44.6\angle -57$
I_9	$16.4\angle -58.5$	$17.9\angle -82$	$13\angle 40$	$10\angle 74$	$36.9\angle 165$
I_{11}	$16.3\angle 26.5$	$18.5\angle -176$	$8\angle -101$	$7\angle 103$	$30.6\angle 36$
I_{13}	$13.2\angle 101.6$	$17.9\angle 74$	$7\angle 58$	$5.9\angle 41$	$26.4\angle -86$
I_{15}	$9.62\angle -171$	$14.7\angle -34$	$5\angle -68$	$5.1\angle -35$	$26.8\angle 148$
I_{17}	$9.02\angle -78.9$	$12.4\angle -134$	$2\angle 71$	$4.5\angle 43$	$28.0\angle 13$
I_{19}	$8.49\angle 0.91$	$11.8\angle 124$	$3\angle -28$	$4.1\angle -29$	$27.3\angle -127$
I_{21}	$6.74\angle 83.3$	$10.6\angle 15$	$1\angle -27$	$3.7\angle -11$	$24.4\angle 92$
I_{23}	$5.84\angle 175$	$8.69\angle -88$	$1\angle -2$	$3.3\angle 32$	$20.0\angle -50$
I_{25}	$5.79\angle -99.4$	$8.31\angle 176$	$1\angle -41$	$3.1\angle -47$	$15.1\angle 172$
I_{27}	$5.03\angle -18.7$	$8.63\angle 68$	$1\angle -2$	$2.9\angle -56$	$10.7\angle 39$
I_{29}	$4.18\angle 70.6$	$8.06\angle -45$	$1\angle -40$	$2.7\angle -9$	$7.81\angle -87$
I_{THD} (%)	110	122	37.8	94.5	148
ΔV_{THD} (%)	0.53	0.73	-0.07	0.28	1.08

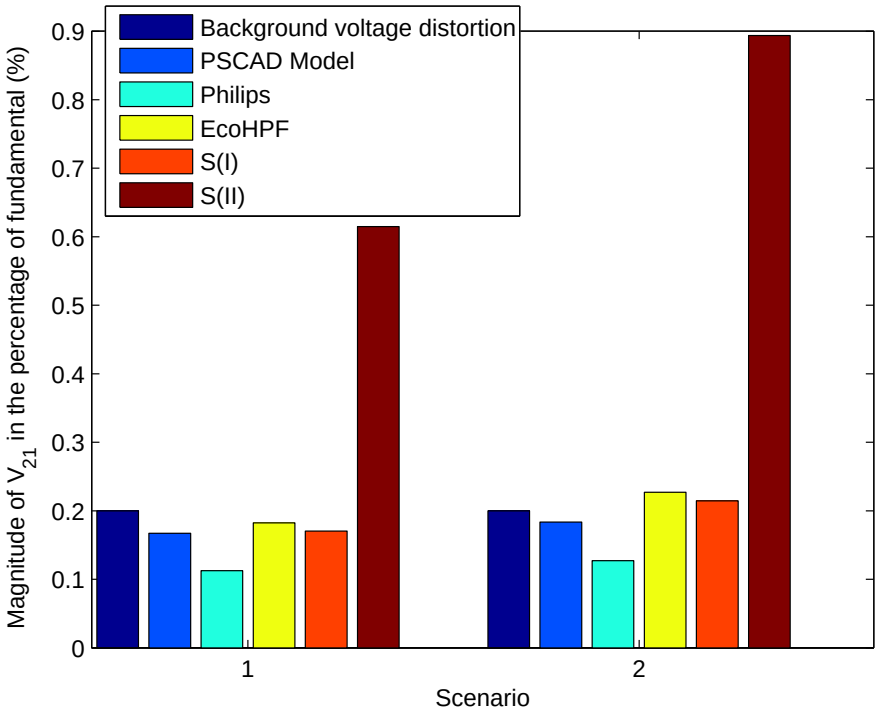

Figure 4.10 Magnitude of Overall V_{21} at the service main when different types of CFL models are applied

Chapter 5

CONCLUSIONS AND FUTURE WORK

5.1 CONCLUSIONS

Compact fluorescent lamps have drawn the attention of utilities and consumers due to their high energy efficiency and long life. However, due to their highly distorted current waveforms, it is necessary to investigate their harmonic impact, particularly when there is widespread deployment in large numbers in the electrical network. The electrical performance of CFLs is related to the type of harmonic filtering or power-factor correction circuit used. A variation of I_{THD} between 5% and 200% has been noticed. In order to perform a detailed analysis of CFL's harmonic behaviour, a 20 Watts CFL circuit with a I_{THD} of 110% has been taken as a general simulation model. Due to the fact that CFLs are often located where the supply voltage are not completely sinusoidal, the harmonic perturbation analysis has been conducted with a wide range of voltage distortions. A CFL admittance tensor matrix has been shown to describe the harmonic interaction between its voltage and current components.

This CFL admittance tensor matrix has been applied to a typical New Zealand distribution network to assess their harmonic impact by assuming five CFLs per house with 28,800 customers (3% of total loading by CFLs in a 100 MVA system). Two common brands of CFL and two fictitious CFL were simulated and compared. The simulation results show a variety of harmonic contribution to their supply terminal voltage distortion. The overall ΔV_{THD} varies from -0.07% to 1.08% on the base of 3.26% V_{THD}. Although there are no other nonlinear loads including in this simulation, it is more likely to be the "worst case" scenario especially when the system is lightly loaded at night. The harmonic limitation criteria which primarily focuses on the 3^{rd} and 5^{th} harmonics allows its current waveform to contain high percentage of higher harmonic components. Therefore, there is a possibility of not only having more voltage distortion at higher frequencies, but also causing interference with other equipment in the ac electrical network, such as ripple relays, if a large number of CFLs deployed are this type. Although the electricity supply system is robust and can tolerate more nonlinear loads than currently exists, the development of standards, as well as the improvement of CFL circuit design are necessary to keep the voltage distortion in the distribution system within the allowable margin.

In summary, this research has successfully achieved the following:

1. Investigated the phase-dependent character of a typical CFL. This was achieved using a simulation model and perturbation analysis in the PSCAD/EMTDC environment.

2. Developed the CFL harmonic tensor model based on the sample data sets from the previous simulation.

3. A harmonic domain algorithm was written for the system being studied and the CFL model incorporated into this to allow the impact of widespread deployment of CFLs to be determined.

5.2 FUTURE WORK

In order to model the voltage dependent character of CFL, the Norton equivalent representation of CFL has been proposed and implemented. For future work, the research can be further extended in terms of computational efficiency and the accuracy of the proposed model. The harmonic perturbation analysis has been performed with a wide range of voltage distortions. These admittance plots indicate that the value of CFL admittance is more subject to the phase angle of the applied voltage rather than its magnitude. This requires the knowledge of busbar voltage V_s where the CFL is going to connected to. The fixed harmonic current injection is also needed to find the estimated status of busbar voltage V_s' when the CFL is in use. Therefore, the perturbation analysis can be performed within a much smaller and more precise phase angle range to enhance the accuracy of the linearized admittance tensor. The inclusion of other commonly used residential nonlinear load models could also be more easily developed and simulated using this type of perturbation analysis and linearization.

Appendix A

COMPLEX FUNCTION AND ITS JACOBIAN

Complex function is a function in which the independent variable and dependent variable are both complex numbers. For any complex function, both the independent variable and dependent variable can be separated into real and imaginary parts. For $I = F(V)$ and $V = V_R + jV_I$,

$$I = F(V) = F_R(V) + iF_I(V) = F_R(V_R, V_I) + iF_I(V_R, V_I) \tag{A.1}$$

where $V_R, V_I \in R$, and $F_R(V)$, $F_I(V)$ are real-valued functions. For the derivatives at some point V_b, we can approach V_b along the real axis toward b, or the imaginary axis towards b by definition as shown in Equation A.2 and A.3 respectively.

$$\begin{aligned}
F'(V) &= \lim_{h\to 0} \frac{F(V+h) - F(V)}{h} \\
&= \lim_{h\to 0} \frac{F_R(V_R+h, V_I) + iF_I(V_R+h, V_I) - [F_R(V_R, V_I) + iF_I(V_R, V_I)]}{h} \\
&= \lim_{h\to 0} \frac{[F_R(V_R+h, V_I) - F_R(V_R, V_I)] + i[F_I(V_R+h, V_I) - F_I(V_R, V_I)]}{h} \\
&= \lim_{h\to 0} \left[\frac{F_R(V_R+h, V_I) - F_R(V_R, V_I)}{h} + i\frac{F_I(V_R+h, V_I) - F_I(V_R, V_I)}{h} \right] \\
&= \frac{\partial F_R}{\partial V_R} + i\frac{\partial F_I}{\partial V_R}
\end{aligned} \tag{A.2}$$

$$\begin{aligned}
F'(V) &= \lim_{h\to 0} \frac{F(V+ih) - F(V)}{ih} \\
&= \lim_{h\to 0} \frac{[F_R(V_R, V_I+h) + iF_I(V_R, V_I+h)] - [F_R(V_R, V_I) + iF_I(V_R, V_I)]}{ih} \\
&= \lim_{h\to 0} \left[\frac{F_R(V_R, V_I+h) - F_R(V_R, V_I)}{ih} + i\frac{F_I(V_R, V_I+h) - F_I(V_R, V_I)}{ih} \right] \\
&= \lim_{h\to 0} \left[\frac{F_I(V_R, V_I+h) - F_I(V_R, V_I)}{h} - i\frac{F_R(V_R, V_I+h) - F_R(V_R, V_I)}{h} \right] \\
&= \frac{\partial F_I}{\partial V_I} - i\frac{\partial F_R}{\partial V_I}
\end{aligned} \tag{A.3}$$

According to Cauchy-Riemann Equation, Equation A.2 and A.3 must be equal if F(V) is defined as complex differentiable. Therefore, we have:

$$\begin{aligned} \frac{\partial F_R}{\partial V_R} + i\frac{\partial F_I}{\partial V_R} &= \frac{\partial F_I}{\partial V_I} - i\frac{\partial F_R}{\partial V_I} \\ \frac{\partial F_R}{\partial V_R} &= \frac{\partial F_I}{\partial V_I} \\ \frac{\partial F_I}{\partial V_R} &= -\frac{\partial F_R}{\partial V_I} \end{aligned}$$

This results the corresponding Jacobian matrix $\begin{bmatrix} \frac{\partial F_R}{\partial V_R}, & \frac{\partial F_R}{\partial V_I} \\ \frac{\partial F_I}{\partial V_R}, & \frac{\partial F_I}{\partial V_I} \end{bmatrix}$ in the form of $\begin{bmatrix} a & -b \\ b & a \end{bmatrix}$. For the linearization of CFL, the relationship between its I and V can be expressed as [23]:

$$I = Y_1 V + Y_2 V^* \tag{A.4}$$

Where $Y_2 \neq 0$ illustrates the linearized admittance is phase dependent. Rearranging equation (A.4), it gives:

$$\begin{aligned} I_R + iI_I &= (Y_{1r} + iY_{1i})(V_R + iV_I) + (Y_{2r} + iY_{2i})(V_R - iV_I) \\ &= \Big(Y_{1r}V_R - Y_{1i}V_I + i(Y_{1i}V_R + Y_{1r}V_I)\Big) + \Big(Y_{2r}V_R + Y_{2i}V_I + i(Y_{2i}V_R - Y_{2r}V_I)\Big) \end{aligned}$$

In a tensor format,

$$\begin{aligned} \begin{bmatrix} \Delta I_r \\ \Delta I_i \end{bmatrix} &= \left(\begin{bmatrix} Y_{1r} & -Y_{1i} \\ Y_{1i} & Y_{1r} \end{bmatrix} + \begin{bmatrix} Y_{2r} & Y_{2i} \\ Y_{2i} & -Y_{2r} \end{bmatrix} \right) \begin{bmatrix} \Delta V_r \\ \Delta V_i \end{bmatrix} \\ &= \begin{bmatrix} Y_{1r} + Y_{2r} & Y_{2i} - Y_{1i} \\ Y_{1i} + Y_{2i} & Y_{1r} - Y_{2r} \end{bmatrix} \begin{bmatrix} \Delta V_r \\ \Delta V_i \end{bmatrix} \\ &= \begin{bmatrix} Y_{11} & Y_{12} \\ Y_{21} & Y_{22} \end{bmatrix} \begin{bmatrix} \Delta V_r \\ \Delta V_i \end{bmatrix} \end{aligned} \tag{A.5}$$

Therefore, the linearized CFL Jacobian Matrix $\begin{bmatrix} \frac{\partial F_R}{\partial V_R}, & \frac{\partial F_R}{\partial V_I} \\ \frac{\partial F_I}{\partial V_R}, & \frac{\partial F_I}{\partial V_I} \end{bmatrix}$ is $\begin{bmatrix} Y_{11} & Y_{12} \\ Y_{21} & Y_{22} \end{bmatrix}$. Where $Y_{11} \neq Y_{22}$, and $Y_{12} \neq -Y_{21}$.

Appendix B

ADMITTANCE TENSOR ELEMENTS CALCULATION

In the harmonic perturbation analysis, the frequency coupling admittance rotates at a constant magnitude with a double step size in the clockwise direction as the applied voltage angle changes from 0 to 2π, with an initial phase angle of β. The admittance circular locus parameters can be expressed in the form of its admittance tensor elements as below [23]:

$$a = \frac{1}{2}(Y_{11} + Y_{22}) \tag{B.1}$$

$$b = \frac{1}{2}(-Y_{12} + Y_{21}) \tag{B.2}$$

$$r = \frac{1}{2}\sqrt{(Y_{11} - Y_{22})^2 + (Y_{12} + Y_{21})^2} \tag{B.3}$$

$$\beta = \tan^{-1}(\frac{Y_{12} + Y_{21}}{Y_{22} - Y_{11}}) \tag{B.4}$$

The aim of this section is to express these tensor elements in terms of the circle parameter in order to provide a reverse approach to find the CFL admittance tensor based on their optimized admittance locus when dealing with the CFL admittance linearization at higher harmonic voltage distortion. From Equation B.1 and B.2, we have:

$$Y_{22} = 2a - Y_{11} \tag{B.5}$$

$$Y_{21} = 2b + Y_{12} \tag{B.6}$$

Substitute Equation B.5 and B.6 into B.3, then Equation B.3 becomes:

$$\begin{aligned} r &= \frac{1}{2}\sqrt{\big(Y_{11} - (2a - Y_{11})\big)^2 + \big(Y_{12} + (2b + Y_{12})\big)^2} \\ &= \frac{1}{2}\sqrt{(2Y_{11} - 2a)^2 + (2Y_{12} + 2b)^2} \\ &= \sqrt{(Y_{11} - a)^2 + (Y_{12} + b)^2} \end{aligned} \tag{B.7}$$

Substitute Equation B.5 and B.6 into B.4, then Equation B.4 becomes:

$$\tan\beta = \frac{Y_{12} + (2b + Y_{12})}{(2a - Y_{11}) - Y_{11}} = \frac{b + Y_{12}}{a - Y_{11}} \tag{B.8}$$

Rearrange B.8, we have:

$$Y_{12} = (a - Y_{11}) \tan\beta - b \tag{B.9}$$

Substitute B.9 into B.7,

$$\begin{aligned}
\sqrt{(Y_{11}-a)^2 + \big((a-Y_{11})\tan\beta - b + b\big)^2} &= r \\
(Y_{11}-a)^2 + \big((a-Y_{11})\tan\beta\big)^2 &= r^2 \\
Y_{11}^2 - 2aY_{11} + a^2 + a^2\tan^2\beta - 2aY_{11}\tan^2\beta + Y_{11}^2\tan^2\beta &= r^2 \\
(1+\tan^2\beta)Y_{11}^2 - 2a(1+\tan^2\beta)Y_{11} + a^2(1+\tan^2\beta) - r^2 &= 0 \\
Y_{11}^2 - 2aY_{11} + (a^2 - \frac{r^2}{\sec^2\beta}) &= 0
\end{aligned} \tag{B.10}$$

Solve Equation B.10 in terms of Y_{11},

$$\begin{aligned}
Y_{11} &= \frac{2a \pm \sqrt{4a^2 - 4\times 1 \times (a^2 - \frac{r^2}{\sec^2\beta})}}{} \\
&= \frac{2a \pm \sqrt{\frac{4r^2}{\sec^2\beta}}}{2} \\
&= \pm\frac{r}{\sec\beta} + a
\end{aligned} \tag{B.11}$$

Substitute B.11 into B.9,

$$\begin{aligned}
Y_{12} &= \big(a - (\pm\frac{r}{\sec\beta} + a)\big)\tan\beta - b \\
&= \mp\frac{r}{\sec\beta} - b
\end{aligned} \tag{B.12}$$

Substitute B.12 into B.6,

$$\begin{aligned}
Y_{21} &= 2b + (\mp\frac{r\tan\beta}{\sec\beta} - b) \\
&= \mp\frac{r\tan\beta}{\sec\beta} + b
\end{aligned} \tag{B.13}$$

Substitute B.11 into B.5,

$$\begin{aligned}
Y_{22} &= 2a - (\pm\frac{r}{\sec\beta} + a) \\
&= \mp\frac{r}{\sec\beta} + a
\end{aligned} \tag{B.14}$$

since $\sec\beta = \frac{1}{\cos\beta}$, where $\beta \neq \pm\frac{\pi}{2}$, if $\beta \in (-\frac{\pi}{2}, \frac{\pi}{2})$,

$$Y_{11} = \frac{r}{\sec\beta} + a \tag{B.15}$$

$$Y_{22} = -\frac{r}{\sec\beta} + a \tag{B.16}$$

elsewhere,

$$Y_{11} = -\frac{r}{\sec\beta} + a \tag{B.17}$$

$$Y_{22} = \frac{r}{\sec\beta} + a \tag{B.18}$$

Also since $\frac{\tan\beta}{\sec\beta} = \frac{\frac{\sin\beta}{\cos\beta}}{\frac{1}{\cos\beta}} = \sin\beta$, if $\beta \in (0, \frac{\pi}{2}) or (\frac{\pi}{2}, \pi)$,

$$Y_{12} = -\frac{r \times \tan\beta}{\sec\beta} - b \tag{B.19}$$

$$Y_{21} = -\frac{r \times \tan\beta}{\sec\beta} + b \tag{B.20}$$

elsewhere,

$$Y_{12} = \frac{r \times \tan\beta}{\sec\beta} - b \tag{B.21}$$

$$Y_{21} = \frac{r \times \tan\beta}{\sec\beta} + b \tag{B.22}$$

REFERENCES

[1] *IEEE Recommended Practices and Requirements for Harmonic Control in Electrical Power Systems*, IEEE Industry Application Society/ Power Engineering Society Std. IEEE Std. 519-1992.

[2] J.M. Crucq and A. Robert, "Statistical approach for harmonics measurements and calculations," *CIRED 10th International Conference on Electricity Distribution*, Vol. 2, pp. 91-96, May 1989.

[3] Y. Baghzouz and O.T. Tan, "Probabilistic modelling of power system harmonics," *IEEE Transactions on Industry Applications*, Vol. IA-23, No. 1, pp. 173-180, January 1987.

[4] W.E. Kazibwe, T.H. Ortmeyer, and M.S.A.A. Hammam, "Summation of probabilistic harmonic vectors," *IEEE Transactions on Power Delivery*, Vol. 4, No. 1, pp. 621-628, January 1989.

[5] D. Xia and G.T. Heydt, "Harmonic power flow studies part I and II," *IEEE Transactions on Power Apparatus and Systems*, Vol. PAS-101, No. 6, pp. 1257-1270, June 1982.

[6] C.D. Callaghan and J. Arrillaga, "Double-iterative algorithm for the analysis of power and harmonic flows at AC/DC convertor terminals," *IEE Proceedings*, Vol. 136, Pt. C, No. 6, pp. 319-324, November 1989.

[7] P.R. Herrick, "Mathematical models for high intensity discharge lamps," *IEEE Transactions on Industry Application*, Vol. IA-16, No. 5, pp. 648-654, September 1980.

[8] E.L. Laskowski and J.F. Donoghue, "A model of a mercury arc lamp's terminal V-I behaviour," *IEEE Transactions on Industry Application*, Vol. IA-17, No. 4, pp. 419-426, July 1981.

[9] W.M. Grady and G.T. Heydt, "Prediction of power system harmonics due to gaseous discharge lighting," *IEEE Transactions on Power Apparatus and Systems*, Vol. PAS-104, No. 3, pp. 554-561, March 1985.

[10] J. Cunill-Sola and M. Salichs, "Study and characterization of waveforms from low-watt (< 25 W) compact fluorescent lamps with electronic ballasts," *IEEE Transactions on Power Delivery*, Vol. 22, No. 4, pp. 2305-2311, October 2007.

[11] J. Arrillaga and N.R. Watson, *"Power System Harmonics,"* 2^{nd} Edition, John Wiley and Sons, Chichester, 2003.

[12] NZCEP 36:1993 *New Zealand electrical code of practice for harmonic levels*, Issued by the Office of the chief electrical inspector, energy and resources division, Ministry of Commerce.

[13] AS/NZS 61000.3.2:2007, *Electromagnetic Compatibility (EMC)-Part 3.2: Limits - Limits for harmonic emissions (equipment input current $\leq$ 16A per phase)*, 2007.

[14] M. Ponce, A.J. Marinez, J. Correa, M. Cotorogea, and J. Arau, "High-efficient integrated electronic ballast for compact fluorescent lamps," *IEEE Transactions on Power Delivery*, Vol. 21, No. 2, pp. 532-542, March 2006.

[15] H.L. Cheng, C.S. Moo, H.C. Yen, T.F. Lin, and S.H. Huang, "Single-switch high-power-factor electronic ballast for compact fluorescent lamps," *Proceedings of 4th IEEE International Conference on Power Electronics and Drive Systems*, Vol. 2, pp. 764-769, October 2001.

[16] R. Prado, M.F. Silva, M. Jungbek, and A.R. Seidel, "Low cost high-power-factor electronic ballast for compact fluorescent lamps," *Proceedings of* 34^{th} *Industry Application Conference Annual Meeting*, Vol. 1, pp. 256-261, October 1999.

[17] Y. Kato, Y. Okamura, T. Kuratani, S. Takahash, and L. Yokozeki, "Development of the back-boost inverter suitable for compact lamps," *Proceedings of* 1^{st} *International Conference on Power Electronics System and Application*, pp. 125-129, November 2004.

[18] P. N. Korovesis, G.A. Vokas, I.F. Gonos, and F.V. Topalis, "Influence of large-scale installation of energy saving lamps on the line voltage distortion of a weak network supplied by photovoltaic station," *IEEE Transactions on Power Delievery*, Vol. 19, No. 4, pp. 1787-1793, October 2004.

[19] T.J. Densem, *"Three Phase Power System Harmonic Penetration,"* PhD Thesis, Department of Electrical and Electronic Engineering, University of Canterbury, Christchurch, New Zealand, 1983.

[20] J. Arrillaga, B.C. Smith, N.R. Watson, and A.R. Wood, *"Power system harmonic analysis,"* John Wiley and Sons, Chichester, 1997.

[21] M. Fauri, "Harmonic modelling of nonlinear load by means of crossed frequency admittance matrix," *IEEE Transactions on Power Systems*, Vol. 12, No. 4, pp. 1632-1638, November 1997.

[22] E. Acha, *"Modelling of power system transformers in the complex conjugate harmonic space,"* PhD Thesis, Department of Electrical and Electronic Engineering, University of Canterbury, Christchurch, New Zealand, 1988.

[23] B.C. Smith, *"A harmonic domain model for the interaction of the HVdc convertor with ac and dc systems,"* PhD Thesis, Department of Electrical and Electronic Engineering, University of Canterbury, Christchurch, New Zealand, 1995.

[24] G.B. Arfken, *"Mathematical methods for physicists,"* 5^{th} Edition, Harcourt/Academic Press, 2001.

[25] G.N. Bathurst, J. Arrillaga, N.R. Watson, and A.R. Wood, "Advanced modelling of the harmonic impedance of AC-DC converters," *IEE Proc.-Gener. Transm. Distrib*, Vol. 149, No. 6, pp. 700-704, November, 2002.

[26] J. Schlabbach, D. Blume, and T. Stephanblome, *"Voltage quality in electrical power systems,"* IEE Power and Energy Series 36, 2001.

[27] D.J. Pileggi, T.J. Gentile, and A.E. Emanuel, "The effect of modern compact fluorescent lights on voltage distortion," *IEEE Transactions on Power Delivery*, Vol. 8, No. 3, pp. 1451-1459, July 1993.

[28] N.R. Watson, T. Scott, and S. Hirsch, "Implications for distribution networks of high penetration of compact fluroescent lamps," *IEEE Transactions on power delivery*, Vol. 24, No. 3, pp. 1521-1528, July 2009.

[29] P.D. Hulme, "Ten years of operational experience with a frequency injection control system," *New Zealand Electrical Journal*, pp. 50, March 1968.

[30] T.B. Norriss and P.S. Bodger, "Ripple control signal interference due to a lightly loaded rural distribution line," *IEE Proceedings*, Vol. 136, Pt. C, No. 6, pp. 401-406, November 1989.

BIBLIOGRAPHY

[1] R. Arseneau and M. Ouellette, "The effects of supply harmonics on the performance of compact fluorescent lamps," *IEEE Transactions on Power Delivery*, Vol. 8, No. 2, pp. 473-479, April, 1993.

[2] F.V. Topalis, "Efficiency of energy saving lamps and harmonic distortion in distribution systems," *IEEE Transactions of Power Delivery*, Vol. 8, No. 4, pp. 2038-2042, October 1993.

[3] N.R. Watson and S. Hirsch, "The impact of compact fluorescent lamps on power quality," *Proceedings of Conference of the Electric Power Supply Industry (CEPSI)*, pp. 416-428, Christchurch, New Zealand, September 1994.

[4] N.R. Watson, D. Chuah, M.B. Dewe, and S. Hirsch, "Harmonic performance of standard and compact fluorescent lamps," *Proc. IPENZ Conference*, pp. 119-122, Palmerston North, New Zealand, 1995.

[5] E. Embriz-Santander, A. Domijian, and C.W. Williams, "A comprehensive harmonic study of electronic ballasts and their effect on a utility's 12 kV, 10 MVA feeder," *IEEE Transactions on Power Delivery*, Vol. 10, No. 3, pp. 1591-1599, July 1995.

[6] R.I. Sasaki, *"The impact of electronic ballast compact fluorescent lighting on power distribution systems,"* M.E. Thesis, School of Electrical Engineering, Purdue University, U.S.A. 1994.

[7] A. Mansoor, M.W. Grady, A.H. Chowdhury, and M.J. Samotyj, "An investigation of harmonics attenuation and diversity among distributed single phase power electronics loads," *IEEE Transactions on Power Delivery*, Vol. 10, No. 1, pp. 467-473, January 1995.

[8] A. Mansoor, M.W. Grady, R.S. Tahallam, M.T. Doyle, and S.D. Krein, "Effect of supply voltage harmonics on the input current of single phase diode bridge rectifier loads," *IEEE Transactions on Power Delivery*, Vol. 10, No. 3, pp. 1416-1422, July 1995.

[9] A. Mansoor, W.M. Grady, P.T. Staats, R.S. Thallam, M.T. Doyle, and M.J. Samotyj, "Predicting the net harmonic currents produced by large numbers of distributed single phase computer loads," *IEEE Transactions on Power Delivery*, Vol. 10, No. 4, pp. 2001-2006, October 1995.

[10] V.J. Gosbell and D.J. Mannix, "Distortion load modelling for distribution system harmonic studies," *Journal of Electrical and Electronics Engineering*, Vol. 19, pp. 51-57, June 1999.

[11] T.M. Zhou, X.Y. Zhu, Y.L. He, W. Cheng, and J. Schlejen, "Preliminary Investigation to the effect of harmonic distortion by CFL on the quality of power systems," Philips Lighting, Fluorescent Development APR.

[12] E. Thunberg and L. Söder, "A Norton approach to distribution network modelling for harmonic studies," *IEEE Transactions on Power Delivery*, Vol. 14, No. 1, pp. 272-277, January 1999.

[13] D.A. Bradley, P.J. Morfee, and L.A. Wilson, "The New Zealand harmonic legislation," *IEE Proceedings*, Vol. 132, Pt. B, No. 4, pp. 177-184, July 1985.

[14] N.R. Watson, "Harmonic assessment of electrical power systems," *International Journal of Energy Technology and Policy*, Vol. 4, No. 1/2, pp. 63-70, 2006.